Does ribosome composition maximize growth rate? The role of RNA instability

Diana Széliová[1*†], **Stefan Müller**[2*†], **Jürgen Zanghellini**[1*†]

[1]Department of Analytical Chemistry, University of Vienna, Austria, EU; [2]Faculty of Mathematics, University of Vienna, Austria, EU

***For correspondence:**
diana.szeliova@univie.ac.at (DZ);
st.mueller@univie.ac.at (SM);
juergen.zanghellini@univie.ac.at (JZ)

[†]All authors contributed equally to this work

Abstract Ribosomes are protein synthesis machines that are central to cellular self-fabrication, and the synthesis time of a ribosome places an upper bound on growth rate. While most cellular enzymes are proteins, ribosomes consist of 1/3 protein and 2/3 RNA (in *E. coli*). Recent research suggests that ribosome composition arises from a trade-off between two "autocatalytic loops", ribosomal protein and RNA polymerase synthesis, respectively.

In this study, we develop a (coarse-grained) mechanistic model of a self-fabricating cell and validate it under various growth conditions. Using resource balance analysis (RBA), we examine how the maximum growth rate varies with ribosome composition, assuming that all kinetic parameters remain independent of ribosome composition. Our model highlights the importance of RNA instability. If we neglect it, RNA synthesis is always "cheaper" than protein synthesis, leading to an RNA-only ribosome at maximum growth rate. However, when we account for RNA turnover, we find that a mixed ribosome composed of RNA and proteins maximizes growth rate.

To account for RNA turnover, we explore two scenarios regarding the activity of RNases. In (a) degradation is proportional to RNA content, whereas in (b) ribosomal proteins cooperatively mitigate RNA instability by protecting it from misfolding and subsequent degradation. In both cases, an increase in ribosomal protein content raises protein synthesis costs while reducing RNA turnover costs. This leads to a mixed ribosome composed of RNA and proteins. However, only in scenario (b), where we consider the cooperative protection of ribosomal RNA by proteins, our model predictions are in qualitative agreement with experimental data under different growth conditions.

Our research offers new mechanistic insights into ribosome biogenesis and evolution. Furthermore, it paves the way for understanding the protein-rich ribosome composition found in archaea and mitochondria.

Contents

Introduction **2**

Results **3**

A small model of a self-fabricating cell 3

Base model recovers linear correlation of RNA to protein ratio with growth rate 5

Base model predicts maximal growth for RNA-only ribosomes 6

rRNA instability leads to maximal growth for mixed ribosomes 7

Extreme conditions increase the optimal protein fraction in (archaeal) ribosomes 9

Discussion **11**
Formal comparison with Kostinski and Reuveni (2020) 14

Methods **15**
Model details 15
Converting constraints from equations/inequalities into matrix form 18
Symbolic analysis of growth rate maximization 19
Numerical growth rate maximization 20

Supplementary figures **25**

Introduction

The ribosome is at the core of any (known) self-replicating organism. In a process called translation, ribosomes read the instructions from messenger ribonucleic acids (mRNAs) to synthesize the corresponding proteins, including ribosomal proteins (rPs). This autocatalytic nature of ribosomes ultimately limits the doubling time of a cell to the period it takes a ribosome to synthesize itself (***Dill et al., 2011***; ***Shore and Albert, 2022***). In *E. coli* this would be $6\,\mathrm{min}$, assuming that the ribosome consists of a 55-protein complex of approximately 7400 amino acids (AAs) that is translated at a speed of $21\,\mathrm{AA/sec}$ (***Bremer and Dennis, 1996***). In fact, even in growth-optimized *E. coli*, that doubling limit remains far from being reached (***Long et al., 2017***). Nonetheless, it has been proposed that ribosomes, not only in *E. coli*, have been subjected to strong selective pressure to minimize their own duplication time in order to speed up the production of all other proteins (***Reuveni et al., 2017***). With this principle in mind, ***Reuveni et al.*** (***2017***) explain why ribosomes have many rPs of similar length.

Ribosomes are structures that have developed over time by adding ribosomal ribonucleic acid (rRNA) and rP around a central core (***Petrov et al., 2015***). This core is considered to be a leftover from ancient translation systems that evolved alongside the genetic code. Different types of ribosomes have evolved in bacteria, archaea, and eukaryotes, but their overall structures are similar within each kingdom (***Melnikov et al., 2018***). For example, the mass of ribosomes in prokaryotes is made up of approximately $63\,\%$ rRNA and $37\,\%$ rPs (***Melnikov et al., 2012***; ***Kurland, 1960***), whereas eukaryotic ribosomes have an equal mass distribution of rRNA and rPs (***Wilson and Cate, 2012***; ***Verschoor et al., 1998***; ***Reuveni et al., 2017***). Thus, the question arises whether there is an evolutionary advantage in having such a high ribonucleic acid (RNA) content.

It has been suggested that the ribosome composition can be understood as a competition for resources between rRNA synthesis and rP synthesis (***Kostinski and Reuveni, 2020***; ***Klumpp, 2020***). In particular, ***Kostinski and Reuveni*** (***2020***) derived two upper bounds on growth rate resulting from two "autocatalytic loops", one for rP production, and one for RNA polymerase (RNAP) and rRNA production. By analyzing allocation data from *E. coli*, they concluded that maximum growth rate occurs at the current ribosome composition of 2/3 RNA and 1/3 protein. However, the specific processes that limit the two autocatalytic processes remained elusive.

Here we aim to provide a mechanistic understanding of these processes. We set up a small (coarse-grained) model of a self-replicating cell and perform resource balance analysis (RBA) (***Goelzer et al., 2015***; ***Molenaar et al., 2009***). In particular, we vary ribosome composition *and* "ribosome allocations" (fractions of ribosomes allocated to the synthesis of different proteins) and maximize growth rate. For simplicity, we assume a constant ribosome mass.

We focus on the primary role of ribosomal proteins, which is stabilizing rRNA (by preventing its degradation or misfolding). Ribosome protein content might also affect other parameters, such as translation rate. Proteins are generally better catalysts than RNA (***Jeffares et al., 1998***), but the ribosome's catalytic core is formed by rRNA (***Tirumalai et al., 2021***) and operates at a relatively slow

(a)

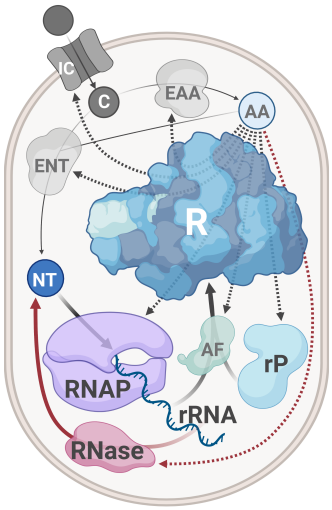

(b)

$$
\begin{array}{c}
 \\ \text{C} \\ \text{AA} \\ \text{NT} \\ \text{rRNA} \\ \text{rP} \\ \text{IC} \\ \text{EAA} \\ \text{ENT} \\ \text{RNAP} \\ \text{RNase} \\ \text{AF} \\ \text{R}
\end{array}
\begin{array}{c}
\begin{array}{ccccccccccccc}
r_{\text{IC}} & r_{\text{EAA}} & r_{\text{ENT}} & r_{\text{RNAP}} & r_{\text{RNase}} & r_{\text{AF}} & s_{\text{IC}} & s_{\text{EAA}} & s_{\text{ENT}} & s_{\text{RNAP}} & s_{\text{RNase}} & s_{\text{AF}} & s_{\text{R}}
\end{array} \\
\begin{pmatrix}
1 & -n_{\text{AA}} & -n_{\text{NT}} & 0 & 0 & 0 & 0 & 0 & 0 & 0 & 0 & 0 & 0 \\
0 & 1 & -1 & 0 & 0 & 0 & -n_{\text{IC}} & -n_{\text{EAA}} & -n_{\text{ENT}} & -n_{\text{RNAP}} & -n_{\text{RNase}} & -n_{\text{AF}} & -n_{\text{rP}} \\
0 & 0 & 1 & -n_{\text{rRNA}} & n_{\text{rRNA}} & 0 & 0 & 0 & 0 & 0 & 0 & 0 & 0 \\
0 & 0 & 0 & 1 & -1 & -1 & 0 & 0 & 0 & 0 & 0 & 0 & 0 \\
0 & 0 & 0 & 0 & 0 & -1 & 0 & 0 & 0 & 0 & 0 & 0 & 1 \\
0 & 0 & 0 & 0 & 0 & 0 & 1 & 0 & 0 & 0 & 0 & 0 & 0 \\
0 & 0 & 0 & 0 & 0 & 0 & 0 & 1 & 0 & 0 & 0 & 0 & 0 \\
0 & 0 & 0 & 0 & 0 & 0 & 0 & 0 & 1 & 0 & 0 & 0 & 0 \\
0 & 0 & 0 & 0 & 0 & 0 & 0 & 0 & 0 & 1 & 0 & 0 & 0 \\
0 & 0 & 0 & 0 & 0 & 0 & 0 & 0 & 0 & 0 & 1 & 0 & 0 \\
0 & 0 & 0 & 0 & 0 & 0 & 0 & 0 & 0 & 0 & 0 & 1 & 0 \\
0 & 0 & 0 & 0 & 0 & 1 & 0 & 0 & 0 & 0 & 0 & 0 & 0
\end{pmatrix}
\end{array}
= \boldsymbol{N}
$$

$$
\begin{pmatrix}
v_{\text{IC}}, & v_{\text{EAA}}, & v_{\text{ENT}}, & v_{\text{RNAP}}, & v_{\text{RNase}}, & v_{\text{AF}}, & w_{\text{IC}}, & w_{\text{EAA}}, & w_{\text{ENT}}, & w_{\text{RNAP}}, & w_{\text{RNase}}, & w_{\text{AF}}, & w_{\text{rP}}
\end{pmatrix} = \boldsymbol{v}^T
$$

Figure 1. A small model of a self-fabricating cell. (a) The cell imports a carbon source (C) and has two types of metabolic enzymes synthesizing amino acids (AA) from the carbon source and nucleotides (NT) from the carbon source and amino acids. The RNA polymerase (RNAP) uses nucleotides to form the ribosomal RNA (rRNA), and the ribosome (R) uses amino acids to synthesize the importer (IC), the metabolic enzymes (EAA, ENT), the ribosomal assembly factors (AF), and the ribosomal protein (rP). Finally, the assembly factors build the ribosome from ribosomal RNA and protein. The processes above constitute the base model. In the extended model, RNase degrades ribosomal RNA (and is synthesized by the ribosome). The additional processes are shown in red. **(b)** The resulting stoichiometric matrix and the corresponding flux vector. Here, s is used for protein *synthesis* reactions (and w for the corresponding fluxes), and r is used for all other reactions (and v for the corresponding fluxes). Additional columns and rows for the extended model are shown in red.

catalytic rate compared to typical enzymes. This suggests that there is little evolutionary pressure to increase the catalytic rate. Furthermore, ribosomes with the lowest protein content, like the *E. coli* ribosome, exhibit the highest translation rates (***Bonven and Gulløv, 1979***; ***Hartl and Hayer-Hartl, 2009***; ***Bremer and Dennis, 2008***). Therefore, we do not consider the impact on translation rate in this study.

We find that the costs of stabilizing rRNA strongly influence the optimal ribosome composition. If we neglect rRNA turnover, our predictions suggest the presence of RNA-only ribosomes (in contrast to experimental evidence). Taking RNA degradation into account, increases its biosynthesis costs, and maximum growth occurs for a mixed (RNA+protein) ribosome.

Results

We introduce a (coarse-grained) mechanistic model of a self-fabricating cell and investigate optimal ribosome composition using RBA. That is, we maximize growth rate under several sets of constraints. We validate the model by predicting RNAP fluxes (rRNA synthesis fluxes), and RNA to protein ratios at different growth rates. Ultimately, we predict maximum growth rate at different ribosome compositions.

A small model of a self-fabricating cell

We consider the small (coarse-grained) model of a self-fabricating cell depicted in ***Figure 1***. The cell imports a carbon source (C) and has two types of metabolic enzymes, one synthesizing amino acids (AA) from the carbon source and the other one synthesizing nucleotides (NT) from the carbon source and amino acids. RNA polymerase (RNAP) uses nucleotides to form the ribosomal RNA (rRNA), while the ribosome (R) uses amino acids to synthesize all proteins, including the im-

Table 1. Constraints used in the "extended" and "base" models (with and without RNA degradation), see ***Figure 1***. In particular, stoichiometric constraints (for the "metabolites" C, AA, NT, rRNA, rP), capacity constraints (for the catalysts IC, EAA, ENT, RNAP, RNase, AF, R), and the (dry) mass constraint. The column 'sign' indicates an equality (=) or inequality (≥) constraint, and the column 'rhs' specifies the right-hand side (a homogeneous or inhomogeneous constraint). Additional columns and rows for the extended model are shown in red.

	v_{IC}	v_{EAA}	v_{ENT}	v_{RNAP}	v_{RNase}	v_{AF}	w_{IC}	w_{EAA}	w_{ENT}	w_{RNAP}	w_{RNase}	w_{AF}	w_{rP}	sign	rhs
C	1	$-n_{\text{AA}}$	$-n_{\text{NT}}$	0	0	0	0	0	0	0	0	0	0	=	0
AA	0	1	-1	0	0	0	$-n_{\text{IC}}$	$-n_{\text{EAA}}$	$-n_{\text{ENT}}$	$-n_{\text{RNAP}}$	$-n_{\text{RNase}}$	$-n_{\text{AF}}$	$-n_{\text{rP}}$	=	0
NT	0	0	1	$-n_{\text{rRNA}}$	n_{rRNA}	0	0	0	0	0	0	0	0	=	0
rRNA	0	0	0	1	-1	-1	0	0	0	0	0	0	0	≥ (=)	0
rP	0	0	0	0	0	-1	0	0	0	0	0	0	1	≥	0
cap IC	$-\mu$	0	0	0	0	0	$k_{\text{IC}}^{\text{cat}}$	0	0	0	0	0	0	≥	0
cap EAA	0	$-\mu$	0	0	0	0	0	$k_{\text{EAA}}^{\text{cat}}$	0	0	0	0	0	≥	0
cap ENT	0	0	$-\mu$	0	0	0	0	0	$k_{\text{ENT}}^{\text{cat}}$	0	0	0	0	≥	0
cap RNAP	0	0	0	$-\mu n_{\text{rRNA}}$	0	0	0	0	0	$\bar{k}_{\text{RNAP}}^{\text{el}}$	0	0	0	≥	0
cap RNase	0	0	0	0	$-\mu n_{\text{rRNA}}$	0	0	0	0	0	$k_{\text{RNase}}^{\text{deg}}$	0	0	≥	0
cap AF	0	0	0	0	0	$-\mu$	0	0	0	0	0	$k_{\text{AF}}^{\text{cat}}$	0	≥	0
cap R	0	0	0	0	0	$\bar{k}_{\text{R}}^{\text{el}}$	$-\mu n_{\text{IC}}$	$-\mu n_{\text{EAA}}$	$-\mu n_{\text{ENT}}$	$-\mu n_{\text{RNAP}}$	$-\mu n_{\text{RNase}}$	$-\mu n_{\text{AF}}$	$-\mu n_{\text{rP}}$	≥ (=)	0
min deg	0	0	0	0	μ	$-k^{\text{deg}}(1-x_{\text{rP}})$	0	0	0	0	0	0	0	≥ (=)	0
(dry) mass	ω_{C}	0	0	0	0	0	0	0	0	0	0	0	0	=	μ

porter (IC), the metabolic enzymes (EAA, ENT), the RNA polymerase and optionally a ribonuclease (RNase), the ribosomal assembly factors (AF), and the ribosomal proteins (rP). Finally, the assembly factors build the ribosome from ribosomal RNA and protein. In a base model, we neglect RNA degradation, whereas in an extended model we consider the enzyme (RNase) that breaks down RNA into nucleotides. We now provide a more formal definition of the two models.

Given the stoichiometric matrix $\boldsymbol{N}$ and the vector of molar masses $\boldsymbol{\omega}$, the dynamic model of cellular growth relates growth rate μ, the vector of (metabolite, RNA, protein, and ribosome) concentrations $\boldsymbol{c}$, and the vector of fluxes ($\boldsymbol{v}$ for "enzymatic" reactions and $\boldsymbol{w}$ for protein synthesis) according to

$$\frac{\mathrm{d}\boldsymbol{c}}{\mathrm{d}t} = \boldsymbol{N}\begin{pmatrix}\boldsymbol{v}\\ \boldsymbol{w}\end{pmatrix} - \mu\,\boldsymbol{c} \qquad \text{and} \qquad \boldsymbol{\omega}^T\boldsymbol{c} = 1.$$

At steady state, growth rate μ and concentrations $\boldsymbol{c}$ are determined by the fluxes $\boldsymbol{v}$ and $\boldsymbol{w}$,

$$\boldsymbol{N}\begin{pmatrix}\boldsymbol{v}\\ \boldsymbol{w}\end{pmatrix} = \mu\,\boldsymbol{c} \geq \boldsymbol{0} \qquad \text{and} \qquad \mu = \boldsymbol{\omega}^T\boldsymbol{N}\begin{pmatrix}\boldsymbol{v}\\ \boldsymbol{w}\end{pmatrix}. \tag{1}$$

To take limited cellular resources into account, we consider capacity constraints for the "enzymatic" fluxes $\boldsymbol{v}$, including transcription (and optionally RNA degradation),

$$v_i \leq k_i^{\text{cat}} c_i, \quad i \in \{\text{IC}, \text{EAA}, \text{ENT}, \text{AF}\}, \tag{2a}$$

$$n_{\text{rRNA}} v_{\text{RNAP}} \leq \bar{k}_{\text{RNAP}}^{\text{el}} c_{\text{RNAP}}, \tag{2b}$$

$$(n_{\text{rRNA}} v_{\text{RNase}} \leq k_{\text{RNase}}^{\text{deg}} c_{\text{RNase}}). \tag{2c}$$

Further, we consider the ribosome capacity constraint for the protein synthesis fluxes $\boldsymbol{w}$,

$$\sum_{i \in \text{Proteins}} n_i w_i \leq \bar{k}_{\text{R}}^{\text{el}} c_{\text{R}}, \quad \text{Proteins} = \{\text{IC}, \text{EAA}, \text{ENT}, \text{RNAP}, (\text{RNase}), \text{AF}, \text{rP}\}. \tag{2d}$$

Here, n_{rRNA} is the number of nucleotides in rRNA, n_i is the number of amino acids in protein i, k_i^{cat} is the corresponding enzyme turnover rate, and $\bar{k}_{\text{RNAP}}^{\text{el}} = k_{\text{RNAP}}^{\text{el}} f_{\text{RNAP}}^{\text{act}}$ and $\bar{k}_{\text{R}}^{\text{el}} = k_{\text{R}}^{\text{el}} f_{\text{R}}^{\text{act}}$ are the effective transcription and translation elongation rates, respectively. $f_{\text{RNAP}}^{\text{act}}$ is the fraction of actively transcribing RNAPs, and $f_{\text{R}}^{\text{act}}$ is the fraction of actively translating ribosomes. As mentioned above, RNase is synthesized optionally and hence put in brackets. By defining the "ribosome allocations",

$$\phi_i^{\text{R}} = \frac{n_i w_i}{\bar{k}_{\text{R}}^{\text{el}} c_{\text{R}}}, \quad i \in \text{Proteins}, \tag{3}$$

that is, the fraction of ribosomes translating a certain protein i, constraint (2d) can be written as

$$\sum_{i \in \text{Proteins}} \phi_i^{\text{R}} \leq 1.$$

We refer to the model given by Equations (1) and (2abd) as the *base* RBA model. Equations (1) and (2), including (2c), define the *extended* RBA model which additionally considers RNA degradation.

Throughout our study, we consider a fixed molar ribosome mass ω_{R}, but variable rRNA and protein content,

$$\omega_{\text{R}} = n_{\text{rRNA}}\, \omega_{\text{NT}} + n_{\text{rP}}\, \omega_{\text{AA}},$$

and we study the influence of ribosome composition on the cell's maximum growth rate, under the constraints specified above. Here, ω_{NT} and ω_{AA} are the molar masses of nucleotides and amino acids, respectively. For convenience, we define the ribosomal protein (mass) fraction

$$x_{\text{rP}} = n_{\text{rP}}\, \frac{\omega_{\text{AA}}}{\omega_{\text{R}}}, \tag{4}$$

and express n_{rRNA} and n_{rP} by x_{rP},

$$n_{\text{rRNA}} = (1 - x_{\text{rP}})\, \frac{\omega_{\text{R}}}{\omega_{\text{NT}}} \quad \text{and} \quad n_{\text{rP}} = x_{\text{rP}}\, \frac{\omega_{\text{R}}}{\omega_{\text{AA}}}.$$

In our analysis, we vary ribosomal protein fraction and maximize growth rate under given constraints. Modeling details can be found in section Methods/subsection Model details, the stoichiometric, capacity, and (dry) mass constraints are summarized in ***Table 1***, and the parameter values are given in ***Table 2***. We used parameters from *E. coli* grown in six different media. Three of them are rich media (Gly+AA, Glc+AA, LB) where amino acids (and nucleotides) are provided so cells only have to express the corresponding transporters instead of the synthesis pathways. In our model, the enzymes ENT and EAA represent lumped pathways for glycolysis and nucleotide / amino acid synthesis, and we only consider one type of transporter. Therefore, to model the changing 'nutrient quality' of the different media (inspired by ***Scott et al.*** (***2010***)), we assume that turnover numbers of EAA and ENT increase with growth rate.

Base model recovers linear correlation of RNA to protein ratio with growth rate

With parameters for *E. coli* in different media (listed in ***Table 2***) and the experimentally observed ribosome composition ($x_{\text{rP}} = 0.36\,\%$), the base model correctly recovers the well-known linear dependence of the RNA to protein ratio and growth rate (***Scott et al., 2010***), see ***Figure 2a***, but not the offset at zero growth rate, since our model does not contain any non-growth associated processes and we assume constant translation elongation rate k_{R}^{el} as in ***Scott et al.*** (***2010***). At low growth rate, k_{R}^{el} decreases, most likely because of the lower availability of the required substrates (***Bremer and Dennis, 2008***; ***Dai et al., 2016***). Interestingly, when we use variable k_{R}^{el}, we observe a nonzero offset (Appendix 1, ***Figure 2***).

To further test the model, we predict RNAP fluxes (v_{RNAP}) at various non-optimal growth rates in glucose minimal medium. In particular, we compute alternative solutions to the system of (in)equalities (1) and (2). (Technically, these solutions are elementary growth vectors (EGVs) as defined in ***Müller et al.*** (***2022***).) We observe three lines (***Figure 2b***). Two lines (in gray) correspond to solutions where either ribosomes or rRNA accumulate (in excess of what is needed) to support growth. In other words, constraints (2d) and (2b) (rows "cap R" and "rRNA" in ***Table 1***) are not limiting. With increasing growth rate, the excess of rRNA and ribosome decreases, reaching zero at the maximum growth rate. The third line (in blue) corresponds to no accumulation of ribosomes or rRNA. In particular, the RNAP flux exactly matches the demand. At maximum growth rate, all lines converge to one optimal value.

For higher growth rates, experimental data are best fit by the line without accumulation of ribosomes or rRNA. In fact, the accumulation of free rRNA in a cell is biologically not realistic as it is bound by rPs already during transcription (***Rodgers and Woodson, 2021***). Furthermore, if rRNA

Table 2. Model parameters for *E. coli* in different media, and for *Thermococcus*. If data for *Thermococcus* was not available, we used *E. coli* parameters from glucose minimal medium. LB, Luria-Bertani medium; Glc+AA, glucose + amino acids medium; Gly+AA, glycerol + amino acids medium; Glc, glucose minimal medium; Gly, glycerol minimal medium; Suc, succinate minimal medium.

Symbol	Name	LB	Glc+AA	Gly+AA	Glc	Gly	Suc	*Thermococcus*	Unit	Source
n_{AA}	ω_{AA}/ω_C	0.61	0.61	1.18	0.61	1.18	0.92	0.61	1	
n_{NT}	$(\omega_{NT}-\omega_{AA})/\omega_C$	1.2	1.2	2.34	1.2	2.34	1.82	1.2	1	
n_{IC}		646						646	1	MC† CPLX-157
n_{EAA}, n_{ENT}		4875						4875	1	Estimate‡
n_{RNAP}		3498						3338	1	***Sutherland and Murakami*** (***2018***); ***Jun et al.*** (***2020***)
n_{AF}		3900						3900	1	Estimate‡
n_{RNase}		813						813	1	MC† EG11259
ω_C	Molar mass carbon source	180	180	92	180	92	118	180	$g\,mol^{-1}$	
ω_{AA}	Molar mass amino acid	109						109	$g\,mol^{-1}$	BNID§ 104877
ω_{NT}	Molar mass nucleotide	324.3						324.3	$g\,mol^{-1}$	BNID§ 104886
ω_R	Molar mass ribosome	2300000						3040000	$g\,mol^{-1}$	***Kostinski and Reuveni*** (***2020***); ***Acca et al.*** (***1993***)
k^{cat}_{IC}	Carbon source import rate	180						180	s^{-1}	BNID§ 114686
k^{cat}_{EAA}	Enzyme turnover number	10.5	8.5	7	5	3.5	2	5	s^{-1}	Estimate*
k^{cat}_{ENT}	Enzyme turnover number	10.5	8.5	7	5	3.5	2	5	s^{-1}	Estimate*
k^{el}_{RNAP}	Transcription elongation rate	85						25	$NT\,s^{-1}$	***Bremer and Dennis*** (***1996***); ***Gehring and Santangelo*** (***2017***)
k^{el}_{R}	Translation elongation rate	21						8.3	$AA\,s^{-1}$	***Bremer and Dennis*** (***1996***), **
k^{cat}_{AF}	Ribosome assembly rate	1/120						1/120	s^{-1}	BNID§ 102321
k^{deg}_{RNase}	RNase degradation rate	88						88	$NT\,s^{-1}$	***Fazal et al.*** (***2015***)
f^{act}_{RNAP}	RNAP activity	0.31	0.242	0.188	0.15	0.144	0.132	0.15	1	***Kostinski and Reuveni*** (***2020***)
f^{act}_{R}	Ribosome activity	0.85						0.85	1	***Bremer and Dennis*** (***2008***)
$\bar{k}^{el}_{RNAP}$	Effective transcription elongation rate $\bar{k}^{el}_{RNAP} = f^{act}_{RNAP} k^{el}_{RNAP}$	26.35	20.57	15.98	12.75	12.24	11.22	12.75	$NT\,s^{-1}$	
$\bar{k}^{el}_{R}$	Effective translation elongation rate $\bar{k}^{el}_{R} = f^{act}_{R} k^{el}_{R}$	17.85						17.85	$AA\,s^{-1}$	
K	Half-saturation constant	0.2						0.2	1	

† MetaCyc ID (***Caspi et al., 2018***).
‡ estimated from an average protein length of 325 amino acids (BNID 108986) and an approximate number of proteins involved in amino acid/nucleotide synthesis (https://www.genome.jp/kegg/), or ribosome assembly (***Choi et al., 2020***).
§ BioNumbers ID (***Milo et al., 2009***).
* To consider the nutrient qualities of the different media, we assumed that k^{cat}_{EAA} and k^{cat}_{ENT} are proportional to the experimental growth rates (Suc: 0.4, Gly: 0.7, Glc:1, Gly+AA:1.4, Glc+AA: 1.7, LB: 2.1 h^{-1}). The growth rates were multiplied by 5 so that the maximum k^{cat}_{EAA} corresponds to the average enzyme turnover rate of 10 (***Bar-Even et al., 2011***).
** An experimentally measured translation rate for *Thermococcus* is unavailable. However, archaeal transcription and translation are likely coordinated, similar to bacteria (***French et al., 2007***; ***Proshkin et al., 2010***). This suggests an upper bound for the translation rate at approximately $25/3 \approx 8.3\,AA\,s^{-1}$.

is expressed in excess of rPs, it is rapidly degraded (***Siehnel and Morgan, 1985***). For the growth rates studied here (0.4-2.1 h^{-1}), the fraction of inactive ribosomes stays roughly constant at 15-20% (***Bremer and Dennis, 1996***, ***2008***; ***Dai et al., 2016***). In our model, we have already incorporated this fraction using the effective translation elongation rate ($\bar{k}^{el}_R = k^{el}_R f^{act}_R$). However, below the growth rate of $\approx 0.5\,h^{-1}$, the fraction of active ribosomes rapidly decreases (***Dai et al., 2016***). Therefore, the disagreement between experimental and simulated data at lower growth rates is probably caused by neglecting other types of RNA. Indeed, RNAP allocation to the synthesis of different types of RNA changes with growth rate (***Bremer and Dennis, 1996***, ***2008***).

Base model predicts maximal growth for RNA-only ribosomes

We study the dependence of maximum growth rate on the ribosomal protein fraction using the base model described above. We find that, for realistic parameters from *E. coli* (***Table 2***), rRNA synthesis is cheaper than protein synthesis for all tested growth conditions (see ***Figure 3a***). Thus, according to our base model, ribosomes should consist of rRNA only. Indeed, it has been suggested that higher growth rates could be achieved if ribosomes were to consist only of rRNA (***Reuveni et al., 2017***).

If we (hypothetically) adjust the parameters to make rRNA synthesis more expensive than protein synthesis (e.g. by decreasing $\bar{k}^{el}_{RNAP}$ or increasing $\bar{k}^{el}_R$), then maximum growth rate is achieved for a protein-only ribosome (Appendix 1, ***Figure 1***). By a symbolic analysis, we can rigorously prove that maximum growth rate is generically attained at an "exclusive" ribosome composition, either

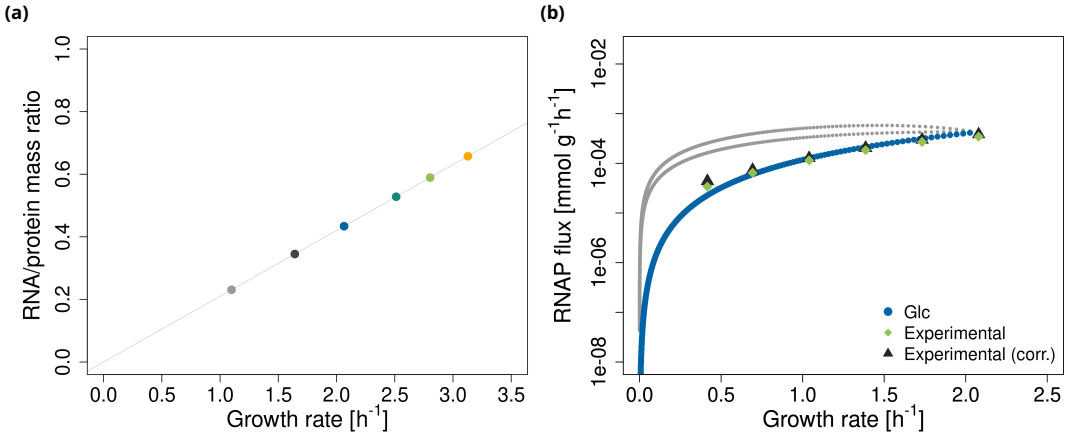

Figure 2. Validation of the base model. **(a)** The model predicts a linear relationship between RNA to protein ratio and growth rate. The points represent the predicted maximum growth rates in six experimental conditions (***Table 2***). The line is a linear fit. **(b)** Alternative RNAP fluxes at different non-optimal growth rates in glucose minimal medium. These are obtained by varying the growth rate step by step from zero to maximum and enumerating all solutions (elementary growth vectors as defined in ***Müller et al.*** (***2022***)) for each growth rate. The grey and blue lines are the alternative solutions. The blue line corresponds to solutions, where rRNA and ribosomes do not accumulate (constraints "rRNA" and "cap R" in ***Table 1*** are limiting). Light green diamonds are experimental data from ***Bremer and Dennis*** (***2008***), black triangles are data from ***Bremer and Dennis*** (***2008***) corrected for rRNA degradation (***Gausing, 1977***). Data was converted to $\mathrm{mmol\,g^{-1}\,h^{-1}}$ with *E. coli* dry masses from ***Bremer and Dennis*** (***2008***).

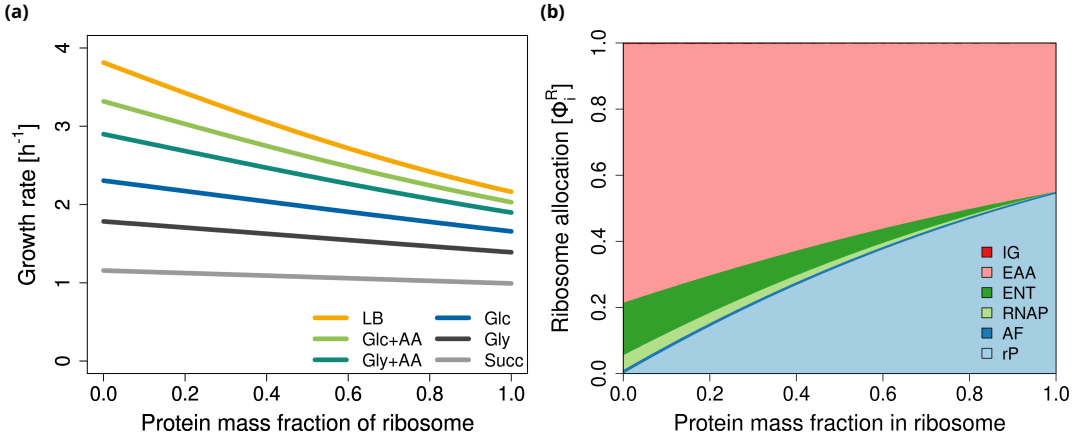

Figure 3. Base model. Maximum growth rate and ribosome allocations as functions of ribosomal protein fraction x_{rP}. **(a)** Maximum growth rate for *E. coli* in six different conditions (see ***Table 2***). **(b)** Ribosome allocations ϕ_i^{R} as defined in Eqn. (3), for glucose minimal medium (Glc).

at $x_{\mathrm{rP}} = 0\%$ or $x_{\mathrm{rP}} = 100\%$, regardless of the parameters (see section Methods/subsection Symbolic analysis of growth rate maximization).

To conclude, RBA with standard capacity constraints does not explain mixed (RNA + protein) ribosomes. Thus, additional constraints are needed.

rRNA instability leads to maximal growth for mixed ribosomes

As one potential explanation, we hypothesize that the different stabilities of rPs and rRNA affect the composition of the ribosome. While proteins are known to be highly stable (***Milo and Phillips,***

2015), rRNA is susceptible to degradation by RNases, which are ubiquitous in cells (***Jain, 2018***). Even at maximum growth, about $10\,\%$ of rRNA is still degraded, and, thus, cannot be incorporated into the ribosome (***Gausing, 1977***; ***Jain, 2018***). Furthermore, rRNA can easily misfold, rendering it inactive and prone to degradation (***Shajani et al., 2011***; ***Rodgers and Woodson, 2021***).

To account for rRNA degradation, we introduce an RNase enzyme that breaks down rRNA into individual nucleotides (NT), via the reaction

$$r_{\text{RNase}}: \ \text{rRNA} \overset{\text{RNase}}{\rightarrow} n_{\text{rRNA}} \cdot \text{NT},$$

see ***Figure 1a***. Since RNases are essential for quality control, we assume some minimum activity and add a minimum degradation rate,

$$v_{\text{RNase}} \geq k^{\text{deg}}(1 - x_{\text{rP}})\, c_{\text{R}}, \tag{5}$$

to the list of constraints (row "min deg" in ***Table 1***). In the simplest case, this rate is directly proportional (with a constant k^{deg}) to the rRNA concentration. The latter is given by the fraction of rRNA in the ribosome concentration, since there is no free rRNA in the cell (***Bremer and Dennis, 1996***). Additionally, $k^{\text{deg}} = k^{\text{deg}}(x_{\text{rP}})$ can be a (monotonically decreasing) function of x_{rP},

$$k^{\text{deg}}(x_{\text{rP}}) = k^{\text{deg}}_{\text{max}} \left(1 - \frac{x^n_{\text{rP}}}{K^n + x^n_{\text{rP}}}\right) \tag{6}$$

modeling the cooperative protection of rRNA by proteins. As for the other enzymes, we add a capacity constraint for the RNase to account for its cost,

$$n_{\text{rRNA}}\, v_{\text{RNase}} \leq k^{\text{deg}}_{\text{RNase}}\, c_{\text{RNase}}, \tag{7}$$

where we use $k^{\text{deg}}_{\text{RNase}} = 88\,\text{NT}\,\text{s}^{-1}$ of an enzyme called RNase R (***Fazal et al., 2015***). The *base* RBA model together with RNA degradation, RNase synthesis, and constraints (5) and (7) constitutes the *extended* RBA model.

Taking rRNA degradation into account leads to maximum growth rates at mixed (RNA+protein) ribosome compositions (***Figure 4***). As it turns out, the assumption of a constant k^{deg} in constraint (5) leads to a very shallow optimum (***Figure 4a***). To account for the stabilizing influence of rPs on the folded structure, we introduce the non-linear (Hill-type) degradation term (Equation (6) with half-saturation $K = 0.2$ and Hill-factors $n = 2$ or $n = 6$), leading to a pronounced optimum, see ***Figure 4b*** and ***Figure 4c***.

In the following, we investigate how the optimal ribosome composition depends on growth conditions.

First, we study growth on glucose minimal medium and adjust $k^{\text{deg}}_{\text{max}}$ such that the optimal ribosome composition matches the experimentally observed value of $x_{\text{rP}} = 0.36$ for *E. coli*. We validate the model for the three types of degradation, and we correctly predict the linear dependence of the RNA to protein ratio on growth rate (Appendix 1, ***Figure 3***). However, RNAP flux predictions are only realistic when assuming strong cooperativity ($n = 6$). For the other two cases, rRNA degradation in the optimum is too high which leads to overestimated RNAP fluxes (Appendix 1, ***Figure 4***).

Second, we predict maximum growth rate as a function of the ribosomal protein fraction in six different growth media. We find that the more proteins cooperate, the less the optimal ribosome composition depends on the growth conditions, see ***Figure 4***(a-c).

Using variable or constant k^{el}_{R} has no impact on the predicted optimal ribosome composition. As in the base model, variable k^{el}_{R} leads to predicted non-zero offset of RNA/protein ratio at zero growth rate (Appendix 1, ***Figure 6***).

Third, to further understand these results, we plot ribosome allocations for glucose minimal medium, see ***Figure 4***(d-f). Interestingly, at low x_{rP}, a significant fraction of ribosomes is allocated to the production of RNAP, whereas with increasing x_{rP}, this ribosome allocation rapidly drops. In the case of the highest cooperativity, allocations at the optimal x_{rP} are comparable to the base RBA model (without RNA degradation), compare ***Figure 4f*** with ***Figure 3b***.

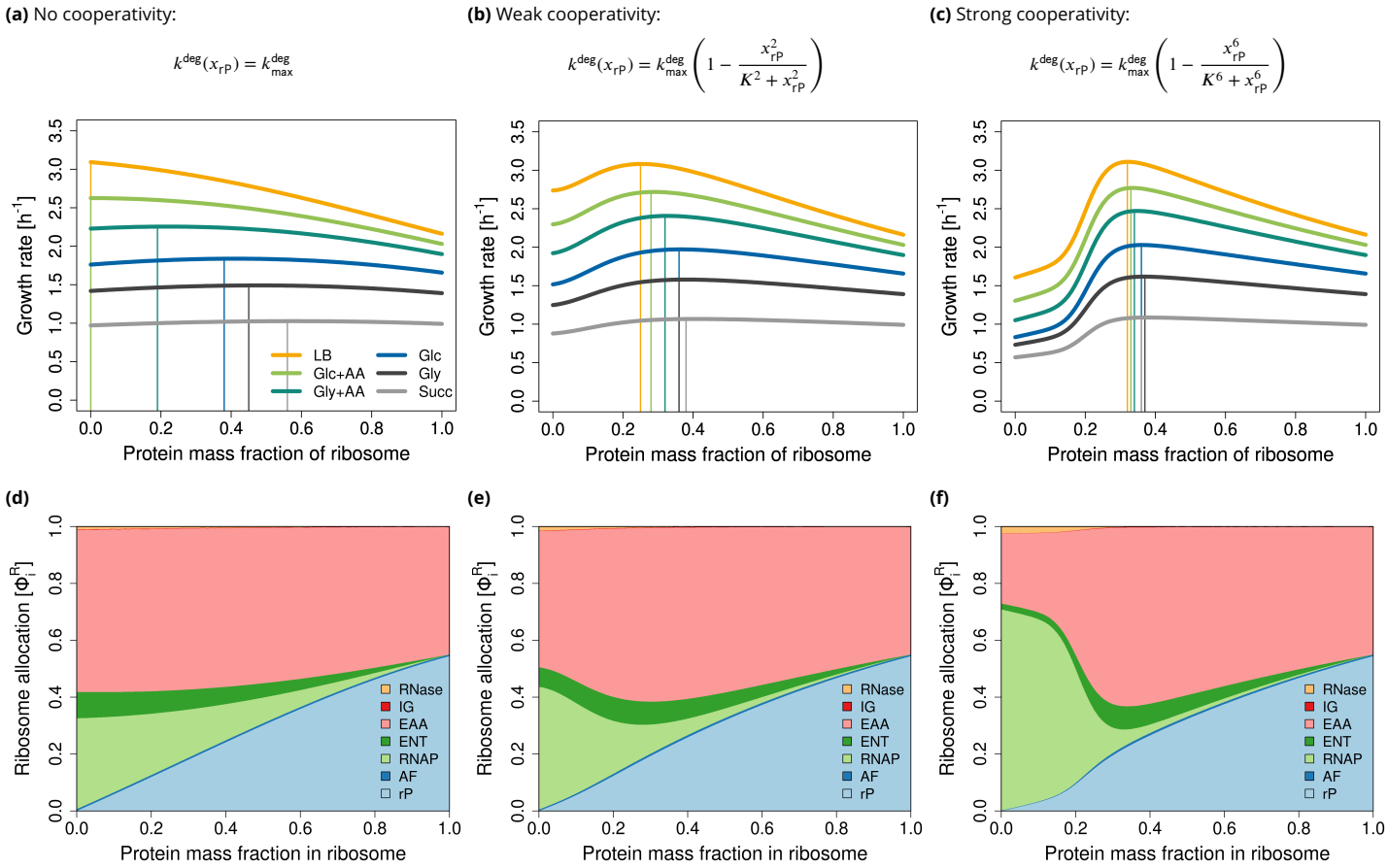

Figure 4. Extended model. Accounting for RNA degradation leads to a mixed (RNA+protein) ribosome composition. **(a-c)** Maximum growth rate of *E. coli* in six different conditions (see ***Table 2***). **(d-f)** Ribosome allocations in glucose minimal medium (Glc). At low protein fractions, rRNA degradation is high, and RNAP (light green) takes up a significant amount of cellular resources.

Finally, we qualitatively predict that the fraction of degraded rRNA decreases with growth rate (***Figure 5***), which is in agreement with experimental observations (***Gausing, 1977***). This effect gets stronger (and closer to experimental data) with higher rP cooperativity. The quantitative disagreement between the experimental and predicted values is probably due to the simplicity of our model. For example, it does not include other types of RNA or regulatory processes, both of which influence RNAP activity. If we consider RNAP allocation to rRNA ($\bar{k}^{el}_{RNAP} = k^{el}_{RNAP} f^{act}_{RNAP} \phi^{RNAP}_{rRNA}$, where ϕ^{RNAP}_{rRNA} is the fraction of RNAP allocated to the synthesis of rRNA), the results get closer to the experimental data (Appendix 1, ***Figure 5***).

Based on these results, we conclude that accounting for RNA degradation and cooperative binding of rP can explain the mixed ribosome composition.

Extreme conditions increase the optimal protein fraction in (archaeal) ribosomes

As a straightforward extension, we explore whether the current model can be adapted to predict the ribosome composition of other organisms. For example, archaeal ribosomes contain $36\,\%$–$50\,\%$ protein (***Acca et al., 1993***), eukaryotic ribosomes $42\,\%$–$50\,\%$ protein (***Wilson and Cate, 2012***; ***Verschoor et al., 1998***; ***Reuveni et al., 2017***), and mitochondrial ribosomes $51\,\%$–$89\,\%$ protein. We ask whether this variability can be explained by efficient resource allocation.

It has been hypothesized that the extra archaeal/eukaryotic ribosomal proteins primarily serve to stabilize the ribosomes (***Kisly and Tamm, 2023***). This may be particularly important for archaea because they commonly live in extreme conditions, such as high temperatures or low pH, which

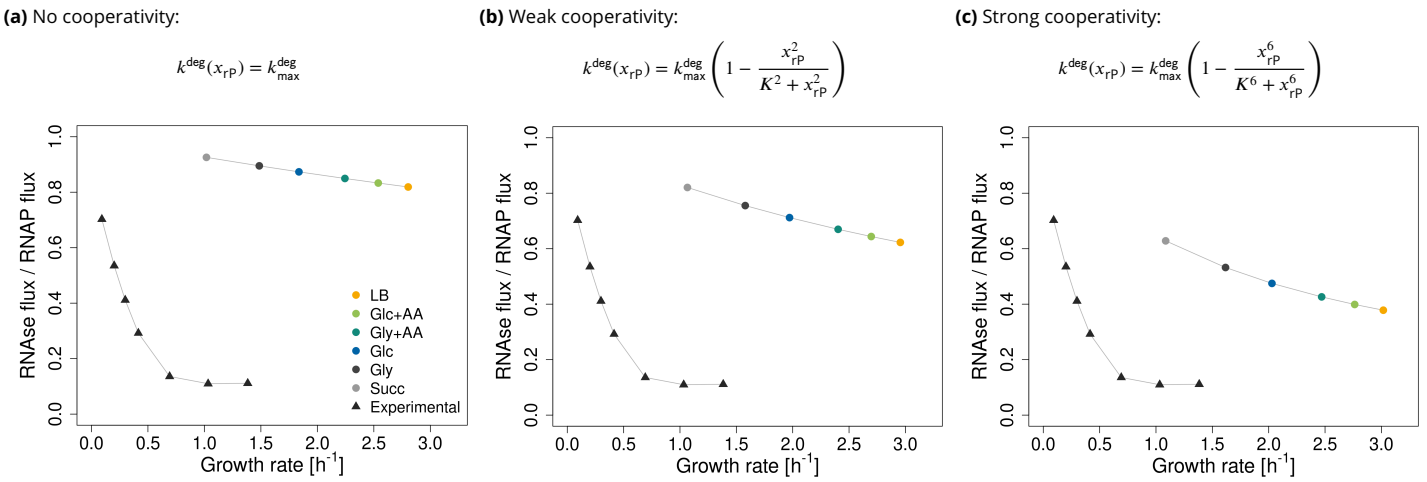

Figure 5. The extended model recapitulates the experimentally observed decrease in the fraction of degraded RNA with increasing growth rate. The circles are the predicted ratios of RNAse fluxes to RNAP fluxes at different conditions. The triangles represent experimental data from ***Gausing*** (***1977***), extracted from the original plot with WebPlotDigitizer (***Rohatgi, 2022***).

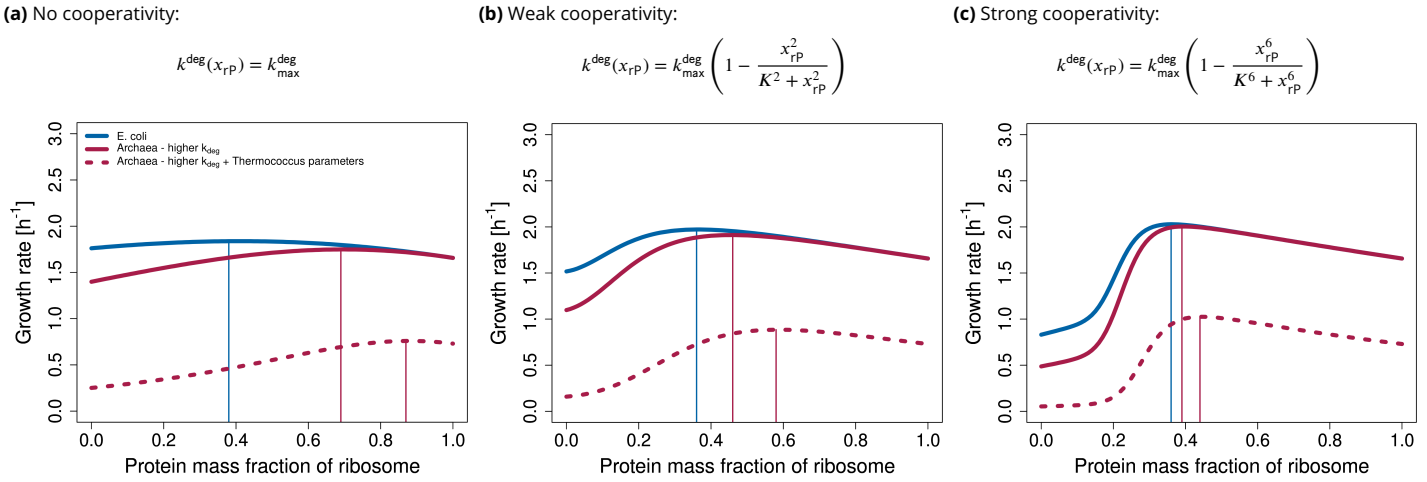

Figure 6. The model can be adjusted to predict archaeal protein-rich ribosome composition. The model was adapted to archaea by increasing k^{deg}_{max} two-fold. The remaining parameters were either kept the same as in *E. coli* (red solid line), or parameters from *Thermococcus* (molecular masses of R and RNAP, transcription and translation rates, see ***Table 2***) were used (red dashed line).

may lead to higher (misfolding and) degradation of RNA. To mitigate this, archaea might need a higher protein content compared to bacteria. It has been shown that the initial steps in ribosome assembly of the thermophilic archaeon *Sufolobus solfataricus* do not require high temperature and likely involve core proteins that are also present in bacteria. However, completing the assembly requires high temperature, suggesting that these proteins have evolved to cope with such extreme conditions (***Altamura et al., 1991***; ***Londei et al., 1986***).

We model this process by increasing k^{deg}_{max} which leads to a higher predicted protein content of the ribosome (***Figure 6***). Similarly to *E. coli*, the higher the cooperativity, the lower the sensitivity of the optimum to the other parameters. Moreover, when using parameters from *Thermococcus* (see ***Table 2***), we observe an increase in ribosomal protein content, in accordance with experimental evidence (***Acca et al., 1993***), and predict a decrease in growth rate.

Discussion

The ribosome is a central player in cellular self-fabrication, placing an upper bound on growth rate. To grow faster, a cell needs more ribosomes which, in turn, requires even more ribosomes to produce themselves. While most catalysts and molecular machines within a cell are proteins, ribosomes stand out by having a significant (mass) fraction of rRNA, playing a catalytic role. The mass fraction of rPs varies across kingdoms, ranging from approximately $36\,\%$ in prokaryotes (***Kurland, 1960***) to around $50\,\%$ in eukaryotes (***Wilson and Cate, 2012***), and even higher in eukaryotic mitochondria, reaching up to $89\,\%$ in *Trypanosoma brucei* (***Moore, 2019***; ***Ramrath et al., 2018***). This prompts the question: what factors determine the ratio of RNA to protein in ribosomes?

The analysis of our base model (without RNA degradation) suggests that RNA-only ribosomes maximize growth rate (***Figure 3a***). This results from the lower cost of rRNA synthesis compared to rP synthesis. It remains true even when one accounts for the synthesis of inactive RNAP and enzymes required for nucleotide synthesis (***Reuveni et al., 2017***), which suggests that the costs of rRNA synthesis and associated processes are underestimated in the base model.

In order to explain a mixed (RNA+protein) ribosome, we consider rRNA degradation in our extended model, thereby increasing the costs for RNA synthesis. While rRNA that is already integrated into a ribosome is stable, nascent RNA may be susceptible to degradation (***Jain, 2018***). Indeed, it has been experimentally observed that even at maximum growth rate, $10\,\%$ of newly synthesized rRNA is degraded (***Gausing, 1977***), and the degradation rate increases if ribosome assembly is delayed (***Jain, 2018***). Furthermore, when rRNA is overexpressed in excess of rPs, it is rapidly degraded (***Siehnel and Morgan, 1985***). Due to the extremely high rates at which rRNA is synthesized, errors become inevitable, necessitating the action of quality control enzymes such as polynucleotide phosphorylase (PNPase) and RNase R to ensure ribosome integrity (***Dos Santos et al., 2018***). The absence of the RNases results in the accumulation of rRNA fragments, ultimately leading to cell death (***Cheng and Deutscher, 2003***; ***Jain, 2018***). In contrast, protein turnover is negligible (***Bremer and Dennis, 2008***), and most ribosomal proteins can exist without rRNA and can be reused (***Reier et al., 2022***; ***Deutscher, 2003***). Therefore, we do not consider protein degradation in our model.

In our resource balance approach, decreasing the RNA content of the ribosome saves resources by reducing RNA turnover. At the same time, protein synthesis costs increase, leading to a mixed (RNA+protein) ribosome at maximum growth rate.

We include RNA degradation in two scenarios. (a) RNA is degraded at a rate proportional to its concentration, or (b) RNA degradation rate decreases non-linearly with ribosomal protein content, since proteins cooperatively protect RNA from degradation (***Shajani et al., 2011***; ***Bowman et al., 2015***; ***Rodgers and Woodson, 2019***). Both versions of the model predict an optimal mixed (RNA+protein) ribosome. However, without considering cooperative protein binding, optimal ribosome compositions depend on growth conditions. Notably, the higher the cooperativity, the closer the predicted RNAP fluxes and the fraction of degraded rRNA are to experimental data. Yet, more experimental data is needed to decide whether ribosome composition in *E. coli* remains truly independent of growth conditions when the bacterium is evolutionarily adapted to a single environment. Based on these results and available experimental evidence for cooperative protein binding (***Rodgers and Woodson, 2019***), we conclude that scenario (b) is more likely.

Our simple model lumps ribosome assembly and RNA degardation and hence allows multiple explanations for the precise mechanism. On the one hand, proteins may stabilize RNA either by blocking the access of RNases to RNA or by preventing misfolding. Intuitively, this could be explained by the fact that RNA molecules are long, and in order to protect them from misfolding and degradation, a certain critical amount of proteins is needed. Folding intermediates can get trapped in misfolded states and are subsequently degraded as a part of quality control. Proteins may help RNA to avoid these kinetic traps (***Bushhouse et al., 2022***; ***Abeysirigunawardena et al., 2017***; ***Shajani et al., 2011***; ***Rodgers and Woodson, 2021***). On the other hand, proteins may increase the rate of

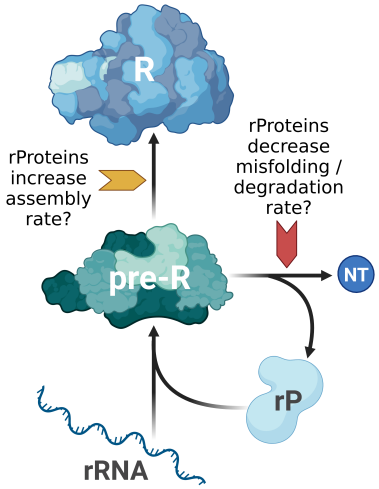

Figure 7. Potential mechanisms by which ribosomal proteins affect the biosynthesis of ribosomes.

ribosome assembly and thereby reduce the number of ribosome intermediates (pre-R in ***Figure 7***). Indeed, it was observed that rRNA can fold to near-native conformation (***K. Lenz et al., 2017***; ***Adilakshmi et al., 2005***). Yet, this process is slower than the protein-supported one, especially for long molecules (***Hyeon and Thirumalai, 2012***; ***Rodgers and Woodson, 2021***).

Throughout the manuscript, we make use of two simplifications:

- As in ***Kostinski and Reuveni*** (***2020***), we consider ribosomes with different compositions, but equal mass. RNA enzymes, known as ribozymes, are generally smaller than proteins and require only a few nucleotides for catalytic activity (***Bernhardt, 2012***). However, such small ribozymes are also inefficient. Increasing their size often improves turnover number, but may impede folding (***Martick and Scott, 2006***; ***Hyeon and Thirumalai, 2012***; ***Jeffares et al., 1998***). Therefore, we consider the case of a large, hard-to-fold, but catalytically efficient RNA-only ribosome.
- We do not consider the effect of protein content on catalytic rates of the ribosomes. Proteins are generally more efficient catalysts than ribozymes (***Jeffares et al., 1998***), yet rRNA is still present in the peptidyl transferase center (***Tirumalai et al., 2021***), and translation rate does not increase in ribosomes from different species which have higher protein content (***Bonven and Gulløv, 1979***; ***Hartl and Hayer-Hartl, 2009***). Furthermore, despite the modest catalytic rate of peptide bond formation, it does not appear to be the rate-limiting step. Given the size of the substrate molecules (mRNA), diffusion may be the limiting factor (***Bernhardt and Tate, 2015***; ***Jeffares et al., 1998***). Therefore, we assume that enhancing ribosome catalytic rate is not the main reason for the addition of proteins. However, it is possible that proteins stabilize the ribosome structure and thereby indirectly ensure efficient peptide bond formation (***Jeffares et al., 1998***).

In future versions of the model, these assumptions can be relaxed. Furthermore, incorporating other types of RNA (mRNA, tRNA) and energy metabolism, or even constructing a genome-scale RBA model (***Hu et al., 2020***), will likely lead to more quantitative predictions of fluxes and growth rate. A strong indication of this is that including a variable RNAP allocation into the model leads to quantitatively better predictions (see Appendix 1, ***Figure 5***). Therefore, in the future, we aim to model RNAP allocation mechanistically. This will involve for example adding other RNA species (mRNA, tRNA), and considering non-specifically bound RNAP which is a significant fraction of RNAP (***Klumpp and Hwa, 2008***).

To better model protein-rich organisms such as archaea, the model could be expanded by including the temperature dependence of rRNA degradation and assembly in more detail. Apart

from $k_{\max}^{\deg}$, other parameters (e.g. K or n in the Hill function) might change too to capture the effects of extreme conditions. Furthermore, the effects of other extreme conditions (such as pH and osmolarity), and the reasons for the variability of archaeal ribosome composition could also be investigated (***Greber et al., 2012***; ***Londei and Ferreira-Cerca, 2021***). However, the predictions of our current model are in agreement with the naive expectation that more proteins are required to keep ribosomes stable in harsh conditions. More experimental data is needed to model the archaeal ribosomes realistically.

Additionally, some extremophilic organisms such as the bacteria *Chloroflexus aurantiacus* or *Fervidobacterium islandicum*, exhibit ribosomes with lower protein content (approximately 40%) compared to extremophilic archaea (50%). It has been suggested that protein-rich ribosomes can be traced back to the oldest phylogenetic lineages, with some ribosomal proteins being lost over time (***Amils et al., 1993***; ***Acca et al., 1993***). Organisms with lower protein content in their ribosomes may have evolved alternative strategies to thrive in extreme conditions. Examples of such strategies include the presence of specific rRNA sequence variants or base modifications, as recently discussed by ***Nissley et al.*** (***2023***).

Moreover, certain archaeal species, such as those from Methanobacteriales or Halobacteriales, have transitioned to milder environmental conditions and subsequently shed unnecessary ribosomal proteins (***Amils et al., 1993***; ***Acca et al., 1993***).

To gain a comprehensive understanding of ribosome evolution in response to changing conditions, a thorough phylogenetic analysis is warranted. This analysis should be complemented by measurements of growth rate, translation rate, RNA degradation rate, among other parameters, to delineate the order of protein loss or gain, and the emergence of sequence variations and base modifications.

In mitochondria, a higher protein content may be advantageous since rP are not made directly in mitochondria, but are imported "for free" from the cytoplasm (***Woellhaf et al., 2014***). In other words, mitochondria can afford to have additional proteins without impacting growth rate and thereby gain additional functionality (e.g. regulation). Indeed, when we allow a "free" import of rP in our model, we observe that the optimum moves towards a protein-rich ribosome (***Figure 8***). However, in order to accurately model mitochondria, it is essential to model the synthesis of cytoplasmic (eukaryotic) ribosomes, several types of RNA polymerases, and the dynamic interaction between host cells and mitochondria. While the cytoplasm provides ribosomal proteins for mitochondria, mitochondria synthesize enzymes of oxidative phosphorylation and provide ATP back to the host cell.

Finally, we need to consider that ribosomal proteins may play other roles in the cells, especially in eukaryotic organisms. Ribosomal proteins participate in translation processes, for example, binding of translation factors, release of tRNA, and translocation. They may also affect the fidelity of translation (***Nikolay et al., 2015***). Furthermore, they play roles in various cellular processes such as cell proliferation, apoptosis, DNA repair, cell migration and others (***Kisly and Tamm, 2023***). These additional functions might have conferred evolutionary fitness advantages. Nevertheless, the primary role of ribosomal proteins seems to be stabilization and folding of rRNA (***Nikolay et al., 2015***; ***Kisly and Tamm, 2023***).

There are still many open questions about ribosome biogenesis and evolution. Our model could guide future experiments. There are a few studies that assessed the effect of individual rP deletions in *E. coli*, for example mutation in S10 increased RNA degradation (***Kuwano et al., 1977***), and mutation in L6 lead to disrupted ribosomal assembly (***Shigeno et al., 2016***). A systematic knock-out screen of all ribosomal proteins could be done (as in ***Shoji et al.*** (***2011***)), complemented with quantification of RNA degradation and misfolding. In case of extremophilic organisms with protein-rich ribosomes, temperature sensitivity could also be assessed. We would expect that deletion of the extra proteins would cause growth defects only at high temperatures. Furthermore, after removal of proteins from archaeal protein-rich ribosomes, laboratory evolution could be performed to see whether growth rate increases beyond wild-type.

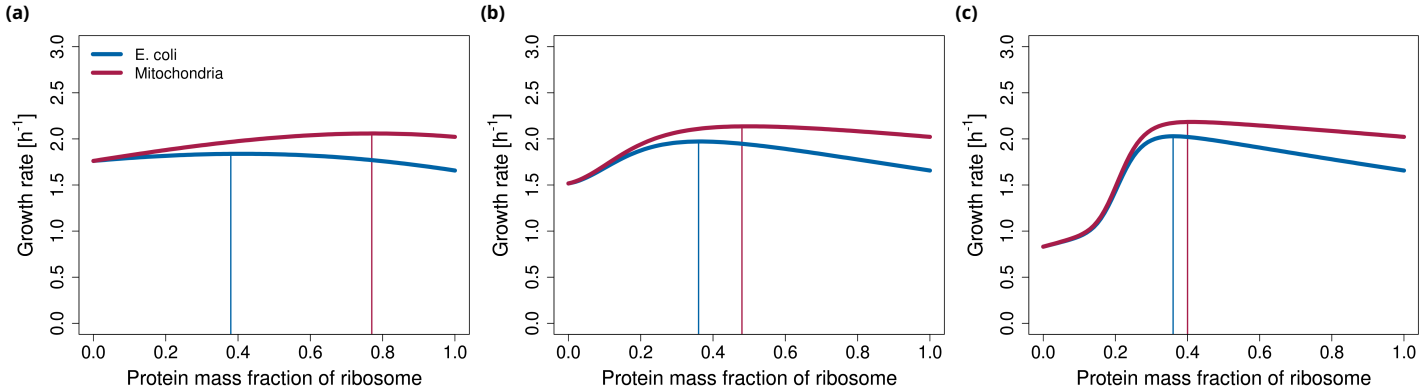

Figure 8. The model can be adjusted to predict mitochondrial protein-rich ribosome composition. All parameters used for the simulation of mitochondria are the same as for *E. coli* in glucose minimal media, except a fraction of rPs can be imported for free from the cytoplasm and does not have to be synthesized. For simplicity, we assumed that 1/3 of rP are imported. (In reality, almost all rP are imported, but mitochondria make additional proteins to provide energy for the whole cell.)

Comprehensive datasets, akin to the work of Bremer and Dennis in 2008 for *E. coli*, should be generated for non-standard organisms by measuring various parameters such as transcription and translation rates, ribosome and RNAP activities, and other relevant factors.

Finally, as mentioned earlier, phylogenetic analysis or ribosome evolution across different species and environments could be done.

Formal comparison with Kostinski and Reuveni (2020)

Our analysis is motivated by the previous work of ***Kostinski and Reuveni*** (***2020***), who understand ribosome composition as a competition between two autocatalytic loops. One loop is responsible for synthesizing rRNA, while the other loop is responsible for rP synthesis, both competing for limited resources. These loops and their constraints, namely, the stoichiometric constraints for rRNA and rP and the capacity constraint for RNAP, are contained in our more detailed RBA model, see ***Table 1***. In addition to these three conditions, ***Kostinski and Reuveni*** (***2020***) make two more assumptions: they fix the "ribosome allocations" $\phi^{\mathrm{R}}_{\mathrm{rP}}$ and $\phi^{\mathrm{R}}_{\mathrm{RNAP}}$ for the synthesis of rP and RNAP, defined in Eqn. (3).

The resulting upper limits on growth rate can be derived easily by considering the synthesis of rRNA and rP, separately.

(rP) The stoichiometric constraint for rP is given by $v_{\mathrm{AF}} \leq w_{\mathrm{rP}}$, see ***Table 1***. Together with the definition of the corresponding ribosome allocation $\phi^{\mathrm{R}}_{\mathrm{rP}} = \frac{\mu\, n_{\mathrm{rP}}\, w_{\mathrm{rP}}}{\bar{k}^{\mathrm{el}}_{\mathrm{R}}\, v_{\mathrm{AF}}}$, this yields

$$\mu \leq \frac{\bar{k}^{\mathrm{el}}_{\mathrm{R}}\, \phi^{\mathrm{R}}_{\mathrm{rP}}}{n_{\mathrm{rP}}}. \tag{8a}$$

(rRNA) The stoichiometric constraint for rRNA and the capacity constraint for RNAP are given by $v_{\mathrm{AF}} \leq v_{\mathrm{RNAP}}$ and $\mu\, n_{\mathrm{rRNA}}\, v_{\mathrm{RNAP}} \leq \bar{k}^{\mathrm{el}}_{\mathrm{RNAP}}\, w_{\mathrm{RNAP}}$, see ***Table 1***. By multiplication, they imply $\mu\, n_{\mathrm{rRNA}}\, v_{\mathrm{AF}} \leq \bar{k}^{\mathrm{el}}_{\mathrm{RNAP}}\, w_{\mathrm{RNAP}}$. Together with the definition of the ribosome allocation $\phi^{\mathrm{R}}_{\mathrm{RNAP}} = \frac{\mu\, n_{\mathrm{RNAP}}\, w_{\mathrm{RNAP}}}{\bar{k}^{\mathrm{el}}_{\mathrm{R}}\, v_{\mathrm{AF}}}$ for the synthesis of RNAP, this yields

$$\mu^2 \leq \frac{\bar{k}^{\mathrm{el}}_{\mathrm{R}}\, \bar{k}^{\mathrm{el}}_{\mathrm{RNAP}}\, \phi^{\mathrm{R}}_{\mathrm{RNAP}}}{n_{\mathrm{rRNA}}\, n_{\mathrm{RNAP}}}. \tag{8b}$$

These upper bounds (8) are Eqns. (2) and (5) in ***Kostinski and Reuveni*** (***2020***), after inserting the effective transcription and translation elongation rate constants $\bar{k}^{\mathrm{el}}_{\mathrm{RNAP}} = k^{\mathrm{el}}_{\mathrm{RNAP}}\, f^{\mathrm{act}}_{\mathrm{RNAP}}\, \phi^{\mathrm{RNAP}}_{\mathrm{rRNA}}$ and $\bar{k}^{\mathrm{el}}_{\mathrm{R}} = k^{\mathrm{el}}_{\mathrm{R}}\, f^{\mathrm{act}}_{\mathrm{R}}$, respectively. Here, $\phi^{\mathrm{RNAP}}_{\mathrm{rRNA}}$ denotes the fraction of RNAP transcribing rRNA (which we assume to equal one in the rest of this work).

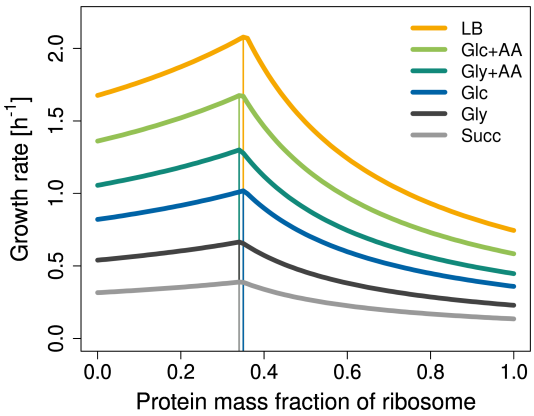

Figure 9. The base RBA model with fixed ribosome allocations and parameters from ***Kostinski and Reuveni*** (***2020***) in multiple growth conditions. For the definition of the ribosome allocations $\phi^{\mathsf{R}}_{\mathsf{rP}}$ and $\phi^{\mathsf{R}}_{\mathsf{RNAP}}$ see Eqn. (3). For the parameter values $(k^{\mathsf{el}}_{\mathsf{R}}, f^{\mathsf{act}}_{\mathsf{R}}, \phi^{\mathsf{R}}_{\mathsf{rP}})$ and $(k^{\mathsf{el}}_{\mathsf{RNAP}}, f^{\mathsf{act}}_{\mathsf{RNAP}}, \phi^{\mathsf{R}}_{\mathsf{RNAP}}, \phi^{\mathsf{RNAP}}_{\mathsf{rRNA}})$, see the original paper.

Using Eqn. (4), the two upper bounds (8) can be written as functions of the rP fraction x_{rP}, namely as

$$\mu \leq \gamma_{\mathsf{rP}} \frac{\phi^{\mathsf{R}}_{\mathsf{rP}}}{x_{\mathsf{rP}}} \quad \text{and} \quad \mu \leq \gamma_{\mathsf{RNAP}} \sqrt{\frac{\phi^{\mathsf{R}}_{\mathsf{RNAP}}}{1 - x_{\mathsf{rP}}}} \tag{9}$$

with constants $\gamma_{\mathsf{rP}}, \gamma_{\mathsf{RNAP}} > 0$. For fixed "ribosome allocations" $\phi^{\mathsf{R}}_{\mathsf{rP}}$ and $\phi^{\mathsf{R}}_{\mathsf{RNAP}}$, the two curves necessarily intersect at some $0 < x^*_{\mathsf{rP}} < 1$, and $\mu(x^*_{\mathsf{rP}})$ is the maximum growth rate allowed by the constraints considered above, namely the stoichiometric constraints for rP and rRNA and the RNAP capacity constraint.

Kostinski and Reuveni (***2020***) interpret Eqns. (9) as a trade-off between rRNA and rP production. This effect arises because they fix the ribosome allocations. In particular, ***Kostinski and Reuveni*** (***2020***) fix $\phi^{\mathsf{R}}_{\mathsf{rP}}$ and $\phi^{\mathsf{R}}_{\mathsf{RNAP}}$ to experimental values for *E. coli* (in multiple growth conditions), and find that maximum growth rate occurs close to the current rP fraction ($x_{\mathsf{rP}} = 36\%$), and the resulting $\mu(x_{\mathsf{rP}})$ is close to the experimental value. If we use their parameters (see ***Table 2***), we can exactly reproduce their results (see ***Figure 9***). Our base model provides an explanation for the protein investment costs, giving a proper mechanistic interpretation to the argument presented by ***Kostinski and Reuveni*** (***2020***). Moreover, it is closer to an evolutionary scenario, where a cell can adjust both ribosome composition x_{rP} and ribosome allocations ϕ^{R}. However, the base model predicts an optimal ribosome that is RNA-only (for realistic parameters), see ***Figure 3a***. This is possible because the ribosome allocations are adjusted according to demand. The ribosome allocations corresponding to varying ribosomal protein fraction are illustrated in ***Figure 3b***. Only the extended model with RNA degradation predicts a mixed (RNA+protein) ribosome at maximum growth rate.

Methods

Our analysis is based on the small model of a self-replicating cell depicted in ***Figure 1*** and described below. Constraints are listed in ***Table 1*** and parameters in ***Table 2***. For an introduction to resource allocation in next-generation models of cellular growth, including the definition of EGVs, see ***Müller et al.*** (***2022***). EGVs were enumerated using the package efmtool 0.2.0 (***Terzer and Stelling, 2008***) in Python 3.8.13. ***Figure 1a*** and ***Figure 7*** were created with `BioRender.com` and the remaining figures with R version 4.1.2. All code is available at https://github.com/diana-sz/RiboComp.

Model details

We consider the small model of a self-fabricating cell depicted in ***Figure 1a*** which contains metabolic reactions and macromolecular synthesis reactions. To take into account the limitation of cellular resources, we use three types of capacity constraints: enzyme capacity constraints limit the rate

of metabolic reactions, the RNAP capacity constraint limits transcription rate, and the ribosome capacity constraint limits the synthesis rates of all proteins (including the ribosomal proteins).

The cell takes up a carbon source (C) via the reaction

$$r_{\mathrm{IC}}: \quad \overset{\mathrm{IC}}{\rightarrow} \mathrm{C},$$

catalyzed by the importer IC, and forms amino acids (AA), nucleotides (NT), and ribosomal RNA (rRNA) via

$$r_{\mathrm{EAA}}: \; n_{\mathrm{AA}} \cdot \mathrm{C} \overset{\mathrm{EAA}}{\rightarrow} \mathrm{AA}, \qquad r_{\mathrm{ENT}}: \; n_{\mathrm{NT}} \cdot \mathrm{C} + \mathrm{AA} \overset{\mathrm{ENT}}{\rightarrow} \mathrm{NT}, \qquad r_{\mathrm{RNAP}}: \; n_{\mathrm{rRNA}} \cdot \mathrm{NT} \overset{\mathrm{RNAP}}{\rightarrow} \mathrm{rRNA},$$

catalyzed by the enzymes EAA, ENT, and the RNA polymerase (RNAP). Ultimately, the ribosome R is built from rRNA and ribosomal protein (rP) via

$$r_{\mathrm{AF}}: \; \mathrm{rRNA} + \mathrm{rP} \overset{\mathrm{AF}}{\rightarrow} \mathrm{R},$$

catalyzed by the assembly factors AF. The processes above are part of the "base model". In an "extended model", ribosomal RNA degrades via

$$r_{\mathrm{RNase}}: \; \mathrm{rRNA} \overset{\mathrm{RNase}}{\rightarrow} n_{\mathrm{rRNA}} \cdot \mathrm{NT},$$

catalyzed by the RNase. Finally, we consider the *synthesis* of all proteins (enzymes and ribosomal protein) via the reactions

$$s_i: \; n_i \cdot \mathrm{AA} \overset{\mathrm{R}}{\rightarrow} i, \quad i \in \mathrm{Proteins} = \{\mathrm{IC}, \mathrm{EAA}, \mathrm{ENT}, \mathrm{RNAP}, (\mathrm{RNase}), \mathrm{AF}, \mathrm{rP}\},$$

catalyzed by the ribosome.

The resulting stoichiometric matrix and the corresponding flux vector are displayed in ***Figure 1b***, and parameter values are given in ***Table 2***. In fact, the stoichiometric matrix can be partitioned into two submatrices,

$$\boldsymbol{N} = \begin{pmatrix} \boldsymbol{N}_{\mathrm{Met}} \\ \boldsymbol{N}_{\mathrm{Cat}} \end{pmatrix},$$

corresponding to the "metabolites" $\mathrm{Met} = \{\mathrm{C}, \mathrm{AA}, \mathrm{NT}, \mathrm{rRNA}, \mathrm{rP}\}$ and the catalysts $\mathrm{Cat} = \mathrm{Enz} \cup \{\mathrm{R}\}$ including the "enzymes" $\mathrm{Enz} = \{\mathrm{IC}, \mathrm{EAA}, \mathrm{ENT}, \mathrm{RNAP}, (\mathrm{RNase}), \mathrm{AF}\}$ and the ribosome. The (total) flux vector, $\boldsymbol{v}_{\mathrm{tot}}$, can be partitioned into two subvectors,

$$\boldsymbol{v}_{\mathrm{tot}} = \begin{pmatrix} \boldsymbol{v} \\ \boldsymbol{w} \end{pmatrix},$$

corresponding to the enzymatic reactions r and the protein synthesis reactions s.

In general, comprehensive models of cellular growth lead to linear (in-)equality systems for the fluxes, and concentrations are determined by fluxes, see ***Box 1***. In the example, we distinguish enzymatic reactions r and protein synthesis reactions s (with corresponding fluxes $\boldsymbol{v}$ and $\boldsymbol{w}$), and further metabolites Met and catalysts Cat, see above. Explicitly, we study the inequality system

$$\begin{pmatrix} \boldsymbol{N}_{\mathrm{Met}} \\ \boldsymbol{N}_{\mathrm{Cat}} \end{pmatrix} \begin{pmatrix} \boldsymbol{v} \\ \boldsymbol{w} \end{pmatrix} \geq \boldsymbol{0}, \quad \boldsymbol{v} \geq \boldsymbol{0}, \; \boldsymbol{w} \geq \boldsymbol{0}, \quad \text{and} \quad \mu = \omega_{\mathrm{C}} v_{\mathrm{IC}},$$

since r_{IC} is the only exchange reaction.

In fact, only $\boldsymbol{N}_{\mathrm{Met}} \binom{\boldsymbol{v}}{\boldsymbol{w}} \geq \boldsymbol{0}$ yields non-trivial constraints, since $\boldsymbol{N}_{\mathrm{Cat}} \binom{\boldsymbol{v}}{\boldsymbol{w}} \geq \boldsymbol{0}$ yields $w_i \geq 0$ for $i \in \mathrm{Enz}$ and $v_{\mathrm{AF}} \geq 0$, already included in $\boldsymbol{v} \geq \boldsymbol{0}$, $\boldsymbol{w} \geq \boldsymbol{0}$. However, $\boldsymbol{N}_{\mathrm{Cat}}$ determines the catalyst concentrations via $\mu\, \boldsymbol{c}_{\mathrm{Cat}} = \boldsymbol{N}_{\mathrm{Cat}} \binom{\boldsymbol{v}}{\boldsymbol{w}}$ or, explicitly,

$$c_i = w_i / \mu, \quad i \in \mathrm{Enz}, \qquad \text{and} \qquad c_{\mathrm{R}} = v_{\mathrm{AF}} / \mu. \tag{10}$$

(Recall that the ribosome is formed by the assembly factors.)

Box 1. Comprehensive models of cellular growth

Comprehensive models of cellular growth (as used in RBA) need not be genome-scale, but involve explicit synthesis reactions for all catalysts. This is in contrast to traditional metabolic models (as used in FBA) which involve an approximate biomass "reaction", thereby fixing biomass composition.

At steady state, the dynamic model of cellular growth yields $\boldsymbol{N}\boldsymbol{v}_{\text{tot}} = \mu\,\boldsymbol{c}$ together with the (dry) mass constraint $\boldsymbol{\omega}^T\boldsymbol{c} = 1$. Thereby, μ is growth rate, $\boldsymbol{v}$ is the vector of fluxes, $\boldsymbol{c}$ is the vector of concentrations, and $\boldsymbol{\omega}$ is the vector of molar masses.

In the constraint-based approach, we consider the (in-)equality system for the fluxes

$$\boldsymbol{N}\boldsymbol{v}_{\text{tot}} \geq \boldsymbol{0}, \quad \boldsymbol{v}_{\text{tot}} \geq \boldsymbol{0}, \quad \text{and} \quad \mu = \boldsymbol{\omega}^T\boldsymbol{N}\boldsymbol{v}_{\text{tot}} = \boldsymbol{\omega}^T\boldsymbol{N}_{\text{exc}}\boldsymbol{v}_{\text{exc}}.$$

Thereby, we assume that all reactions have a given direction, and we use the fact that growth rate is determined by the exchange reactions, cf. ***Müller et al.*** (***2022***).

Finally, concentrations are determined by fluxes via $\boldsymbol{c} = \boldsymbol{N}\boldsymbol{v}_{\text{tot}}/\mu$. In particular, concentrations of catalysts are used to formulate additional capacity constraints.

Now, catalyst concentrations are used to formulate capacity constraints (for importer, metabolic enzymes, and assembly factors),

$$v_i \leq k_i^{\text{cat}}\,c_i, \quad i \in \{\text{IC}, \text{EAA}, \text{ENT}, \text{AF}\} \subset \text{Enz}, \tag{11a}$$

where k_i^{cat} are the corresponding enzyme turnover numbers. The capacity constraints for the RNA polymerase, (optionally the RNase), and the ribosome are given by

$$n_{\text{rRNA}}\,v_{\text{RNAP}} \leq \bar{k}_{\text{RNAP}}^{\text{el}}\,c_{\text{RNAP}}, \qquad (n_{\text{rRNA}}\,v_{\text{RNase}} \leq k_{\text{RNase}}^{\text{deg}}\,c_{\text{RNase}}), \tag{11b}$$

and

$$\sum_{i\in\text{Proteins}} n_i\,w_i \leq \bar{k}_{\text{R}}^{\text{el}}\,c_{\text{R}}, \tag{11c}$$

respectively. Here, n_{rRNA} is the number of nucleotides in rRNA, and n_i is the number of amino acids in protein i, cf. the stoichiometric coefficients in ***Figure 1b***. Further, $\bar{k}_{\text{RNAP}}^{\text{el}} = k_{\text{RNAP}}^{\text{el}} f_{\text{RNAP}}^{\text{act}}$ and $\bar{k}_{\text{R}}^{\text{el}} = k_{\text{R}}^{\text{el}} f_{\text{R}}^{\text{act}}$ are the effective transcription and translation elongation rate constants, respectively, and $k_{\text{RNase}}^{\text{deg}}$ is the RNA degradation rate constant.

Finally, catalyst concentrations are expressed by corresponding fluxes in all capacity constraints (11) via Eqns. (10). The stoichiometric, capacity, and (dry) mass constraints described so far are summarized in ***Table 1***, and the parameter values are given in ***Table 2***.

In particular, after using (10), the ribosome capacity constraint (11c) takes the form

$$\sum_{i\in\text{Proteins}} \mu\,n_i\,w_i \leq \bar{k}_{\text{R}}^{\text{el}}\,v_{\text{AF}},$$

which suggests the definition of "ribosome allocations" (ribosome fractions translating certain proteins),

$$\phi_i^{\text{R}} = \frac{\mu\,n_i\,w_i}{\bar{k}_{\text{R}}^{\text{el}}\,v_{\text{AF}}}, \quad i \in \text{Proteins}.$$

Obviously, $\sum_{i\in\text{Proteins}} \phi_i^{\text{R}} \leq 1$. Instead of varying the protein synthesis fluxes $\boldsymbol{w}$, one may vary v_{AF} (the ribosome synthesis flux) and the (vector of) ribosome allocations $\boldsymbol{\phi}^{\text{R}}$.

Throughout this work, we consider a fixed ribosome mass, but variable ribosomal RNA and protein content,

$$\omega_{\text{R}} = n_{\text{rRNA}}\,\omega_{\text{NT}} + n_{\text{rP}}\,\omega_{\text{AA}},$$

where n_{rRNA} and n_{rP} are the numbers of nucleotides and amino acids in rRNA and rP, respectively. We define the ribosomal protein (mass) fraction

$$x_{\mathrm{rP}} = n_{\mathrm{rP}} \frac{\omega_{\mathrm{AA}}}{\omega_{\mathrm{R}}},$$

and express n_{rRNA} and n_{rP} by x_{rP},

$$n_{\mathrm{rRNA}} = (1 - x_{\mathrm{rP}}) \frac{\omega_{\mathrm{R}}}{\omega_{\mathrm{NT}}} \quad \text{and} \quad n_{\mathrm{rP}} = x_{\mathrm{rP}} \frac{\omega_{\mathrm{R}}}{\omega_{\mathrm{AA}}}.$$

For variable ribosomal protein fraction x_{rP} (from 0 to 100%), we maximize growth rate (by varying fluxes under the given constraints).

Converting constraints from equations/inequalities into matrix form

For convenience, we describe how to obtain the constraints in ***Table 1*** from the equations/inequalities given in the subsection "Model details" above.

Capacity constraints

The capacity constraints for enzymes have the form

$$v_i \leq k_i^{\mathrm{cat}} c_i, \quad i \in \{\mathrm{IC}, \mathrm{EAA}, \mathrm{ENT}, \mathrm{AF}\}.$$

Concentrations c_i can be expressed by synthesis fluxes w_i via $c_i = w_i/\mu$, and hence

$$v_i \leq k_i^{\mathrm{cat}} w_i/\mu.$$

Multiplying by μ and bringing all terms to one side, we get

$$-\mu v_i + k_i^{\mathrm{cat}} w_i \geq 0$$

or, in vector form,

$$\begin{pmatrix} -\mu & k_i^{\mathrm{cat}} \end{pmatrix} \begin{pmatrix} v_i \\ w_i \end{pmatrix} \geq 0.$$

The row vector is the non-zero part of the row in ***Table 1*** that specifies the capacity constraint cap i, for $i \in \{\mathrm{IC}, \mathrm{EAA}, \mathrm{ENT}, \mathrm{AF}\}$.

For the RNAP and RNase capacity constraints (cap RNAP and cap RNase, respectively), we further have $k_i^{\mathrm{cat}} = \bar{k}_{\mathrm{RNAP}}^{\mathrm{el}}/n_{\mathrm{rRNA}}$ and $k_i^{\mathrm{cat}} = k_{\mathrm{RNase}}^{\mathrm{deg}}/n_{\mathrm{rRNA}}$. Hence,

$$\begin{pmatrix} -\mu n_{\mathrm{rRNA}} & \bar{k}_{\mathrm{RNAP}}^{\mathrm{el}} \end{pmatrix} \begin{pmatrix} v_{\mathrm{RNAP}} \\ w_{\mathrm{RNAP}} \end{pmatrix} \geq 0$$

and

$$\begin{pmatrix} -\mu n_{\mathrm{rRNA}} & k_{\mathrm{RNase}}^{\mathrm{deg}} \end{pmatrix} \begin{pmatrix} v_{\mathrm{RNase}} \\ w_{\mathrm{RNase}} \end{pmatrix} \geq 0.$$

Finally, for the ribosome capacity constraint, $\sum_{i \in \mathrm{Proteins}} n_i w_i \leq \bar{k}_{\mathrm{R}}^{\mathrm{el}} c_{\mathrm{R}}$, ribosome concentration c_{R} can be expressed by assembly flux v_{AF} via $c_{\mathrm{R}} = v_{\mathrm{AF}}/\mu$. Ultimately,

$$\bar{k}_{\mathrm{R}}^{\mathrm{el}} v_{\mathrm{AF}} - \sum_{i \in \mathrm{Proteins}} \mu n_i w_i \geq 0.$$

After expanding the sum, this yields the row in ***Table 1*** that specifies cap R.

Minimum degradation rate

Minimum degradation rate is enforced by

$$v_{\mathrm{RNase}} \geq k^{\mathrm{deg}} (1 - x_{\mathrm{rP}}) c_{\mathrm{R}}.$$

As before, ribosome concentration is expressed by assembly flux,

$$v_{\mathrm{RNase}} \geq k^{\mathrm{deg}} (1 - x_{\mathrm{rP}}) v_{\mathrm{AF}}/\mu,$$

which can be written as in ***Table 1***,

$$\begin{pmatrix} \mu & -k^{\mathrm{deg}}(1 - x_{\mathrm{rP}}) \end{pmatrix} \begin{pmatrix} v_{\mathrm{RNase}} \\ v_{\mathrm{AF}} \end{pmatrix} \geq 0.$$

Box 2. The determinant method

(In-)homogeneous linear equality and inequality constraints on a vector $x \in \mathbb{R}^n$ can be summarized by matrices $A' \in \mathbb{R}^{m' \times n}$, $A'' \in \mathbb{R}^{m'' \times n}$ and vectors $b' \in \mathbb{R}^{m'}$, $b'' \in \mathbb{R}^{m''}$ as

$$A'x = b', \quad A''x \geq b''.$$

After homogenization, one obtains

$$B'x' = 0, \quad B''x' \geq 0 \quad \text{for} \quad x' = \begin{pmatrix} x \\ 1 \end{pmatrix} \in \mathbb{R}^{n+1},$$

$$\text{where} \quad B' = \left(A', -b'\right) \in \mathbb{R}^{m' \times (n+1)}, \quad B'' = \left(A'', -b''\right) \in \mathbb{R}^{m'' \times (n+1)}.$$

Assume that, for a particular x, all inequality constraints are active, that is, $B''x' = 0$. Then,

$$Bx' = 0,$$

$$\text{where} \quad B = \begin{pmatrix} B' \\ B'' \end{pmatrix} \in \mathbb{R}^{(m'+m'') \times (n+1)}.$$

If B is square (that is, if $m' + m'' = n + 1$), then

$$\det B = 0,$$

that is, its determinant is zero.
In the main text, we consider particular (sub-)sets of constraints on the vector of fluxes v_{tot} in the form $A'v_{\text{tot}} = b'$, $A''v_{\text{tot}} \geq b''$ and assume that, at maximum growth rate, all constraints are active, and the resulting matrix B is square. We compute its determinant, set it to zero, and determine the maximum growth rate from the resulting (quadratic) equation.

Dry mass constraint

As stated in Box 1, growth rate is determined by the exchange fluxes. Indeed, in the dry mass constraint $\boldsymbol{\omega}^T \boldsymbol{c} = 1$, concentrations $\boldsymbol{c}$ can be expressed by fluxes $\boldsymbol{v}_{\text{tot}}$ via $\boldsymbol{N}\boldsymbol{v}_{\text{tot}} = \mu \boldsymbol{c}$ and hence $\boldsymbol{\omega}^T \boldsymbol{N}\boldsymbol{v}_{\text{tot}} = \mu$. Since internal reactions are mass-balanced, only exchange reactions contribute to growth,

$$\boldsymbol{\omega}^T \boldsymbol{N}_{\text{exc}} \boldsymbol{v}_{\text{exc}} = \mu.$$

In our small model, the only exchange reaction is carbon import and hence

$$\omega_{\text{C}} v_{\text{IC}} = \mu.$$

Symbolic analysis of growth rate maximization

In order to confirm our numerical results, we also perform a symbolic analysis of growth rate maximization.

The "base model" involves five stoichiometric constraints (for the species C, AA, NT, RNAP, rP), six capacity constraints (for the reactions catalyzed by IC, EAA, ENT, RNAP, AF, R), and one (dry) mass constraint, cf. ***Table 1*** (without the columns and rows in red). They define a linear equality and inequality system with 12 constraints (either $\geq$ or $=$) for 11 fluxes and 1 right-hand side.

We apply the determinant method introduced in ***Box 2*** to the resulting matrix $B \in \mathbb{R}^{12 \times 12}$, and we find

$$0 = \det B \sim \left(\left[\frac{n_{\text{IC}}}{k_{\text{IC}}^{\text{cat}}} \frac{\omega_{\text{NT}}}{\omega_{\text{G}}} + \frac{n_{\text{EAA}}}{k_{\text{EAA}}^{\text{cat}}} + \frac{n_{\text{ENT}}}{k_{\text{ENT}}^{\text{cat}}} + \frac{n_{\text{RNAP}}}{\bar{k}_{\text{RNAP}}^{\text{el}}} \right] n_{\text{rRNA}} + \frac{n_{\text{AF}}}{k_{\text{AF}}^{\text{cat}}} \right) \mu^2 + \left(\bar{k}_{\text{R}}^{\text{el}} \left[\frac{n_{\text{IC}}}{k_{\text{IC}}^{\text{cat}}} \frac{\omega_{\text{AA}}}{\omega_{\text{G}}} + \frac{n_{\text{EAA}}}{k_{\text{EAA}}^{\text{cat}}} \right] + n_{\text{rP}} \right) \mu - \bar{k}_{\text{R}}^{\text{el}}.$$

Using ribosomal protein fraction and rescaling time,

$$n_{\mathrm{rRNA}} = (1 - x_{\mathrm{rP}})\frac{\omega_{\mathrm{R}}}{\omega_{\mathrm{NT}}}, \quad n_{\mathrm{rP}} = x_{\mathrm{rP}}\frac{\omega_{\mathrm{R}}}{\omega_{\mathrm{AA}}}, \quad \text{and} \quad \hat{\mu} = \frac{\mu}{\bar{k}_{\mathrm{R}}^{\mathrm{el}}}\frac{\omega_{\mathrm{R}}}{\omega_{\mathrm{AA}}},$$

we obtain a quadratic equation for maximum growth rate,

$$0 = \left(\alpha + \beta(1 - x_{\mathrm{rP}})\right)\hat{\mu}^2 + \left(\gamma + x_{\mathrm{rP}}\right)\hat{\mu} - 1 \tag{12}$$

with

$$\begin{aligned}
\alpha &= \bar{k}_{\mathrm{R}}^{\mathrm{el}}\frac{n_{\mathrm{AF}}}{k_{\mathrm{AF}}^{\mathrm{cat}}}\left(\frac{\omega_{\mathrm{AA}}}{\omega_{\mathrm{R}}}\right)^2 \\
\beta &= \bar{k}_{\mathrm{R}}^{\mathrm{el}}\left[\frac{n_{\mathrm{IC}}}{k_{\mathrm{IC}}^{\mathrm{cat}}}\frac{\omega_{\mathrm{AA}}}{\omega_{\mathrm{G}}} + \left(\frac{n_{\mathrm{EAA}}}{k_{\mathrm{EAA}}^{\mathrm{cat}}} + \frac{n_{\mathrm{ENT}}}{k_{\mathrm{ENT}}^{\mathrm{cat}}} + \frac{n_{\mathrm{RNAP}}}{\bar{k}_{\mathrm{RNAP}}^{\mathrm{el}}}\right)\frac{\omega_{\mathrm{AA}}}{\omega_{\mathrm{NT}}}\right]\frac{\omega_{\mathrm{AA}}}{\omega_{\mathrm{R}}} \\
\gamma &= \bar{k}_{\mathrm{R}}^{\mathrm{el}}\left[\frac{n_{\mathrm{IC}}}{k_{\mathrm{IC}}^{\mathrm{cat}}}\frac{\omega_{\mathrm{AA}}}{\omega_{\mathrm{G}}} + \frac{n_{\mathrm{EAA}}}{k_{\mathrm{EAA}}^{\mathrm{cat}}}\right]\frac{\omega_{\mathrm{AA}}}{\omega_{\mathrm{R}}}.
\end{aligned}$$

For fixed $x_{\mathrm{rP}} \in [0, 1]$, the quadratic equation (12) has one positive solution $\hat{\mu}(x_{\mathrm{rP}})$. To show that it is monotone in x_{rP}, we differentiate (12) and set $\mathrm{d}\hat{\mu}/\mathrm{d}x_{\mathrm{rP}} = 0$. We get

$$0 = -\beta\hat{\mu}^2 + \hat{\mu}$$

which has the positive solution $\hat{\mu} = 1/\beta$. Insertion into (12) yields

$$0 = (\alpha + \beta)\left(\frac{1}{\beta}\right)^2 + \gamma\frac{1}{\beta} - 1 =: \varepsilon,$$

which does not depend on x_{rP}. In fact, if $\varepsilon = 0$, then $\hat{\mu}$ is constant. Otherwise, $\hat{\mu}$ is strictly monotone in x_{rP} (decreasing if $\varepsilon > 0$ and increasing if $\varepsilon < 0$).

For realistic parameters, $\hat{\mu}$ is decreasing (and $\hat{\mu} < 1/\beta$).

Approximation. For realistic parameters, $\alpha \ll \beta \leq 1$, and for all $x_{\mathrm{rP}} \in [0, 1]$, we may set $\alpha = 0$ in the quadratic equation (12): For $x_{\mathrm{rP}} \to 0$, obviously $\alpha + (1 - x_{\mathrm{rP}})\beta \to \alpha + \beta \approx \beta$. For $x_{\mathrm{rP}} \to 1$, the crucial quantity $4(\alpha + (1 - x_{\mathrm{rP}})\beta)/(\gamma + x_{\mathrm{rP}})^2 \to 4\alpha/(1 + \gamma)^2 \ll 1$, and the quadratic term can be neglected.

Numerical growth rate maximization

We fix growth rate and solve the system of equations (1) and (2) using efmtool 0.2.0 (***Terzer and Stelling, 2008***) in Python 3.8.13. We use bisection search to find the highest growth rate that still enables a feasible solution.

References

Abeysirigunawardena SC, Kim H, Lai J, Ragunathan K, Rappé MC, Luthey-Schulten Z, Ha T, Woodson SA. Evolution of protein-coupled RNA dynamics during hierarchical assembly of ribosomal complexes. Nature communications. 2017; 8(1):492.

Acca M, Bocchetta M, Ceccarelli E, Creti R, Stetter KO, Cammarano P. Updating Mass and Composition of Archaeal and Bacterial Ribosomes. Archaeal-like Features of Ribosomes from the Deep-Branching Bacterium Aquifex pyrophilus. Systematic and Applied Microbiology. 1993 Feb; 16(4):629–637. https://www.sciencedirect.com/science/article/pii/S0723202011803346, doi: 10.1016/S0723-2020(11)80334-6.

Adilakshmi T, Ramaswamy P, Woodson SA. Protein-independent Folding Pathway of the 16S rRNA 5' Domain. Journal of Molecular Biology. 2005 Aug; 351(3):508–519. https://www.sciencedirect.com/science/article/pii/S0022283605006704, doi: 10.1016/j.jmb.2005.06.020.

Altamura S, Caprini E, Sanchez M, Londei P. Early assembly proteins of the large ribosomal subunit of the thermophilic archaebacterium Sulfolobus. Identification and binding to heterologous rRNA species. Journal of Biological Chemistry. 1991; 266(10):6195–6200.

Amils R, Cammarano P, Londei P. Translation in archaea. In: *New Comprehensive Biochemistry*, vol. 26 Elsevier; 1993.p. 393–438.

Bar-Even A, Noor E, Savir Y, Liebermeister W, Davidi D, Tawfik DS, Milo R. The Moderately Efficient Enzyme: Evolutionary and Physicochemical Trends Shaping Enzyme Parameters. Biochemistry. 2011; 50(21):4402–4410. https://doi.org/10.1021/bi2002289, doi: 10.1021/bi2002289, pMID: 21506553.

Bernhardt HS. The RNA world hypothesis: the worst theory of the early evolution of life (except for all the others) a. Biology direct. 2012; 7(1):1–10.

Bernhardt HS, Tate WP. A Ribosome Without RNA. Frontiers in Ecology and Evolution. 2015; 3:129.

Bonven B, Gulløv K. Peptide chain elongation rate and ribosomal activity in Saccharomyces cerevisiae as a function of the growth rate. Molecular and General Genetics MGG. 1979; 170(2):225–230.

Bowman JC, Hud NV, Williams LD. The ribosome challenge to the RNA world. Journal of Molecular Evolution. 2015; 80(3):143–161.

Bremer H, Dennis P. Modulation of chemical composition and other parameters of the cell by growth rate. Escherichia coli and Salmonella: cellular and molecular biology. American Society for Microbiology,. 1996; p. 1553–1568.

Bremer H, Dennis PP. Modulation of chemical composition and other parameters of the cell at different exponential growth rates. EcoSal Plus. 2008; 3(1):10–1128.

Bushhouse DZ, Choi EK, Hertz LM, Lucks JB. How does RNA fold dynamically? Journal of molecular biology. 2022; p. 167665.

Caspi R, Billington R, Fulcher CA, Keseler IM, Kothari A, Krummenacker M, Latendresse M, Midford PE, Ong Q, Ong WK, et al. The MetaCyc database of metabolic pathways and enzymes. Nucleic acids research. 2018; 46(D1):D633–D639.

Cheng ZF, Deutscher MP. Quality control of ribosomal RNA mediated by polynucleotide phosphorylase and RNase R. Proceedings of the National Academy of Sciences. 2003; 100(11):6388–6393. https://www.pnas.org/doi/abs/10.1073/pnas.1231041100, doi: 10.1073/pnas.1231041100.

Choi E, Jeon H, Oh JI, Hwang J. Overexpressed L20 rescues 50S ribosomal subunit assembly defects of bipA-deletion in Escherichia coli. Frontiers in microbiology. 2020; 10:2982.

Dai X, Zhu M, Warren M, Balakrishnan R, Patsalo V, Okano H, Williamson JR, Fredrick K, Wang YP, Hwa T. Reduction of translating ribosomes enables Escherichia coli to maintain elongation rates during slow growth. Nature microbiology. 2016; 2(2):1–9.

Deutscher MP. Degradation of stable RNA in bacteria. Journal of Biological Chemistry. 2003; 278(46):45041–45044.

Dill KA, Ghosh K, Schmit JD. Physical limits of cells and proteomes. Proceedings of the National Academy of Sciences. 2011; 108:17876–17882. doi: 10.1073/pnas.1114477108, publisher: Proceedings of the National Academy of Sciences.

Dos Santos RF, Quendera AP, Boavida S, Seixas AF, Arraiano CM, Andrade JM. Major 3'–5' exoribonucleases in the metabolism of coding and non-coding RNA. Progress in molecular biology and translational science. 2018; 159:101–155.

Fazal FM, Koslover DJ, Luisi BF, Block SM. Direct observation of processive exoribonuclease motion using optical tweezers. Proceedings of the National Academy of Sciences. 2015; 112(49):15101–15106.

French SL, Santangelo TJ, Beyer AL, Reeve JN. Transcription and Translation are Coupled in Archaea. Molecular Biology and Evolution. 2007 Jan; 24(4):893–895. https://academic.oup.com/mbe/article-lookup/doi/10.1093/molbev/msm007, doi: 10.1093/molbev/msm007.

Gausing K. Regulation of ribosome production in Escherichia coli: synthesis and stability of ribosomal RNA and of ribosomal protein messenger RNA at different growth rates. Journal of molecular biology. 1977; 115(3):335–354.

Gehring AM, Santangelo TJ. Archaeal RNA polymerase arrests transcription at DNA lesions. Transcription. 2017 Jun; 8(5):288–296. https://www.ncbi.nlm.nih.gov/pmc/articles/PMC5703245/, doi: 10.1080/21541264.2017.1324941.

Goelzer A, Muntel J, Chubukov V, Jules M, Prestel E, Nölker R, Mariadassou M, Aymerich S, Hecker M, Noirot P, et al. Quantitative prediction of genome-wide resource allocation in bacteria. Metabolic engineering. 2015; 32:232–243.

Greber BJ, Boehringer D, Godinic-Mikulcic V, Crnkovic A, Ibba M, Weygand-Durasevic I, Ban N. Cryo-EM structure of the archaeal 50S ribosomal subunit in complex with initiation factor 6 and implications for ribosome evolution. Journal of molecular biology. 2012; 418(3-4):145–160.

Hartl FU, Hayer-Hartl M. Converging concepts of protein folding in vitro and in vivo. Nature structural & molecular biology. 2009; 16(6):574–581.

Hu XP, Dourado H, Schubert P, Lercher MJ. The protein translation machinery is expressed for maximal efficiency in Escherichia coli. Nature communications. 2020; 11(1):5260.

Hyeon C, Thirumalai D. Chain length determines the folding rates of RNA. Biophysical journal. 2012; 102(3):L11–L13.

Jain C. Role of ribosome assembly in Escherichia coli ribosomal RNA degradation. Nucleic acids research. 2018; 46(20):11048–11060.

Jeffares DC, Poole AM, Penny D. Relics from the RNA world. Journal of molecular evolution. 1998; 46:18–36.

Jun SH, Hyun J, Cha JS, Kim H, Bartlett MS, Cho HS, Murakami KS. Direct binding of TFEα opens DNA binding cleft of RNA polymerase. Nature communications. 2020; 11(1):1–12.

Kisly I, Tamm T. Archaea/eukaryote-specific ribosomal proteins-guardians of a complex structure. Computational and Structural Biotechnology Journal. 2023; .

Klumpp S. Speed Limit for Cell Growth. Physics. 2020; 13:108. doi: 10.1103/PhysRevLett.125.028103.

Klumpp S, Hwa T. Growth-rate-dependent partitioning of RNA polymerases in bacteria. Proceedings of the National Academy of Sciences. 2008; 105(51):20245–20250. doi: 10.1073/pnas.0804953105.

Kostinski S, Reuveni S. Ribosome Composition Maximizes Cellular Growth Rates in E. coli. Physical Review Letters. 2020; 125(2):028103. doi: 10.1103/PhysRevLett.125.028103.

Kurland CG. Molecular characterization of ribonucleic acid from *Escherichia coli* ribosomes: I. Isolation and molecular weights. Journal of Molecular Biology. 1960; 2(2):83–91.

Kuwano M, Taniguchi H, Ono M, Endo H, Ohnishi Y. An Escherichia coli K12 mutant carrying altered ribosomal protein (S10). Biochemical and Biophysical Research Communications. 1977; 75(1):156–162.

K Lenz T, M Norris A, V Hud N, Dean Williams L. Protein-free ribosomal RNA folds to a near-native state in the presence of Mg 2+. RSC Advances. 2017; 7(86):54674–54681. https://pubs.rsc.org/en/content/articlelanding/2017/ra/c7ra08696b, doi: 10.1039/C7RA08696B, zSCC: NoCitationData[s0].

Londei P, Ferreira-Cerca S. Ribosome biogenesis in archaea. Frontiers in Microbiology. 2021; 12:1476.

Londei P, Teuudò J, Acca M, Cammarano P, Amils R. Total reconstitation of active large ribosomal subunlts of the tbermoaddophllk arcfaaebacterium Sulfolobus solfataricus. Nucleic acids research. 1986; 14(5):2269–2285.

Long CP, Gonzalez JE, Cipolla RM, Antoniewicz MR. Metabolism of the fast-growing bacterium Vibrio natriegens elucidated by 13C metabolic flux analysis. Metabolic engineering. 2017; 44:191–197.

Martick M, Scott WG. Tertiary contacts distant from the active site prime a ribozyme for catalysis. Cell. 2006; 126(2):309–320.

Melnikov S, Ben-Shem A, Garreau de Loubresse N, Jenner L, Yusupova G, Yusupov M. One core, two shells: bacterial and eukaryotic ribosomes. Nature Structural & Molecular Biology. 2012 Jun; 19(6):560–567. https://www.nature.com/articles/nsmb.2313, doi: 10.1038/nsmb.2313.

Melnikov S, Manakongtreecheep K, Söll D. Revising the structural diversity of ribosomal proteins across the three domains of life. Molecular Biology and Evolution. 2018; 35(7):1588–1598.

Milo R, Jorgensen P, Moran U, Weber G, Springer M. BioNumbers—the database of key numbers in molecular and cell biology. Nucleic Acids Research. 2009 10; 38(suppl_1):D750–D753. https://doi.org/10.1093/nar/gkp889, doi: 10.1093/nar/gkp889.

Milo R, Phillips R. Cell biology by the numbers. Garland Science; 2015.

Molenaar D, Van Berlo R, De Ridder D, Teusink B. Shifts in growth strategies reflect tradeoffs in cellular economics. Molecular systems biology. 2009; 5(1):323.

Moore PB. In Which the Deity Attempts To Make a Ribose-Free Ribosome. Biochemistry. 2019; 58(6):431–432. https://doi.org/10.1021/acs.biochem.8b01191, doi: 10.1021/acs.biochem.8b01191.

Müller S, Széliová D, Zanghellini J. Elementary vectors and autocatalytic sets for resource allocation in next-generation models of cellular growth. PLoS computational biology. 2022; 18(2):e1009843.

Nikolay R, van den Bruck D, Achenbach J, Nierhaus KH. Ribosomal proteins: role in ribosomal functions. eLS. 2015; p. 1–12.

Nissley AJ, Penev PI, Watson ZL, Banfield JF, Cate JH. Rare ribosomal RNA sequences from archaea stabilize the bacterial ribosome. Nucleic Acids Research. 2023; 51(4):1880–1894.

Petrov AS, Gulen B, Norris AM, Kovacs NA, Bernier CR, Lanier KA, Fox GE, Harvey SC, Wartell RM, Hud NV, et al. History of the ribosome and the origin of translation. Proceedings of the National Academy of Sciences. 2015; 112(50):15396–15401.

Proshkin S, Rahmouni AR, Mironov A, Nudler E. Cooperation Between Translating Ribosomes and RNA Polymerase in Transcription Elongation. Science. 2010 Apr; 328(5977):504–508. https://www.science.org/doi/10.1126/science.1184939, doi: 10.1126/science.1184939.

Ramrath DJ, Niemann M, Leibundgut M, Bieri P, Prange C, Horn EK, Leitner A, Boehringer D, Schneider A, Ban N. Evolutionary shift toward protein-based architecture in trypanosomal mitochondrial ribosomes. Science. 2018; 362(6413):eaau7735.

Reier K, Lahtvee PJ, Liiv A, Remme J. A conundrum of r-protein stability: unbalanced stoichiometry of r-proteins during stationary phase in Escherichia coli. Mbio. 2022; 13(5):e01873–22.

Reuveni S, Ehrenberg M, Paulsson J. Ribosomes are optimized for autocatalytic production. Nature. 2017; 547(7663):293–297.

Rodgers ML, Woodson SA. Transcription Increases the Cooperativity of Ribonucleoprotein Assembly. Cell. 2019; 179(6):1370–1381.e12. https://www.sciencedirect.com/science/article/pii/S0092867419312280, doi: https://doi.org/10.1016/j.cell.2019.11.007.

Rodgers ML, Woodson SA. A roadmap for rRNA folding and assembly during transcription. Trends in Biochemical Sciences. 2021; 46(11):889–901.

Rohatgi A, Webplotdigitizer: Version 4.6; 2022. https://automeris.io/WebPlotDigitizer, last accessed on 2017-11-30.

Scott M, Gunderson CW, Mateescu EM, Zhang Z, Hwa T. Interdependence of cell growth and gene expression: origins and consequences. Science. 2010; 330(6007):1099–1102.

Shajani Z, Sykes MT, Williamson JR. Assembly of Bacterial Ribosomes. Annual Review of Biochemistry. 2011 Jul; 80(1):501–526. https://www.annualreviews.org/doi/10.1146/annurev-biochem-062608-160432, doi: 10.1146/annurev-biochem-062608-160432.

Shigeno Y, Uchiumi T, Nomura T. Involvement of ribosomal protein L6 in assembly of functional 50S ribosomal subunit in Escherichia coli cells. Biochemical and Biophysical Research Communications. 2016; 473(1):237–242.

Shoji S, Dambacher CM, Shajani Z, Williamson JR, Schultz PG. Systematic chromosomal deletion of bacterial ribosomal protein genes. Journal of molecular biology. 2011; 413(4):751–761.

Shore D, Albert B. Ribosome biogenesis and the cellular energy economy. Current Biology. 2022; 32(12):R611–R617.

Siehnel RJ, Morgan EA. Unbalanced rRNA gene dosage and its effects on rRNA and ribosomal-protein synthesis. Journal of bacteriology. 1985; 163(2):476–486.

Sutherland C, Murakami KS. An introduction to the structure and function of the catalytic core enzyme of Escherichia coli RNA polymerase. EcoSal Plus. 2018; 8(1).

Terzer M, Stelling J. Large-scale computation of elementary flux modes with bit pattern trees. Bioinformatics. 2008; 24(19):2229–2235.

Tirumalai MR, Rivas M, Tran Q, Fox GE. The peptidyl transferase center: a window to the past. Microbiology and Molecular Biology Reviews. 2021; 85(4):e00104–21.

Verschoor A, Warner JR, Srivastava S, Grassucci RA, Frank J. Three-dimensional structure of the yeast ribosome. Nucleic Acids Research. 1998 Jan; 26(2):655–661. https://academic.oup.com/nar/article-lookup/doi/10.1093/nar/26.2.655, doi: 10.1093/nar/26.2.655.

Wilson DN, Cate JHD. The Structure and Function of the Eukaryotic Ribosome. Cold Spring Harbor Perspectives in Biology. 2012 May; 4(5):a011536. http://cshperspectives.cshlp.org/content/4/5/a011536, doi: 10.1101/cshperspect.a011536.

Woellhaf MW, Hansen KG, Garth C, Herrmann JM. Import of ribosomal proteins into yeast mitochondria. Biochemistry and Cell Biology. 2014; 92(6):489–498.

Appendix 1

Supplementary figures

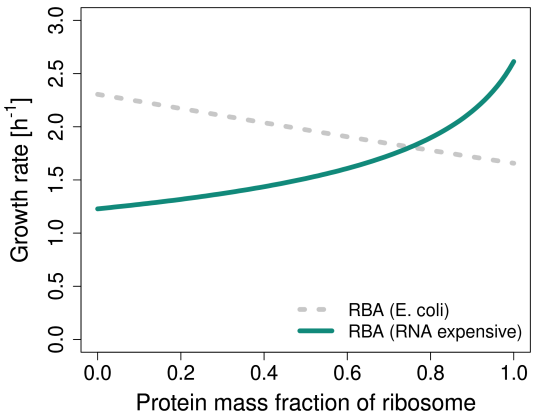

Appendix 1 Figure 1. RBA with realistic parameters for glucose minimal medium from ***Table 2*** (grey curve) vs. RBA with parameters that make RNA more expensive than proteins ($k^{el}_{RNAP} = 8.5\,\mathrm{NT\,s^{-1}}$, $k^{el}_{R} = 63\,\mathrm{AA\,s^{-1}}$, $n_{RNAP} = 52470$; green curve).

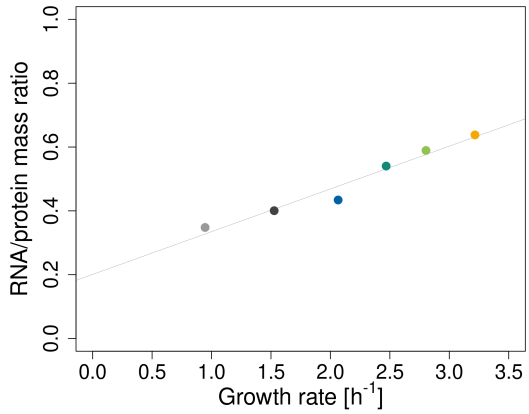

Appendix 1 Figure 2. Using variable translation elongation rate (k^{el}_{R}) leads to a predicted non-zero offset of RNA/protein ratio at zero growth rate. The points are predicted RNA/protein ratios for *E. coli* in six different conditions. The line is a linear fit. The used translation elongation rates (k^{el}_{R}) are: Succ, 12; Gly, 16.83; Glc, 21 ; Gly+AA, 20.17; Glc+AA, 21; LB, 22.25 $\mathrm{AA\,s^{-1}}$. The remaining parameters are listed in ***Table 2***.

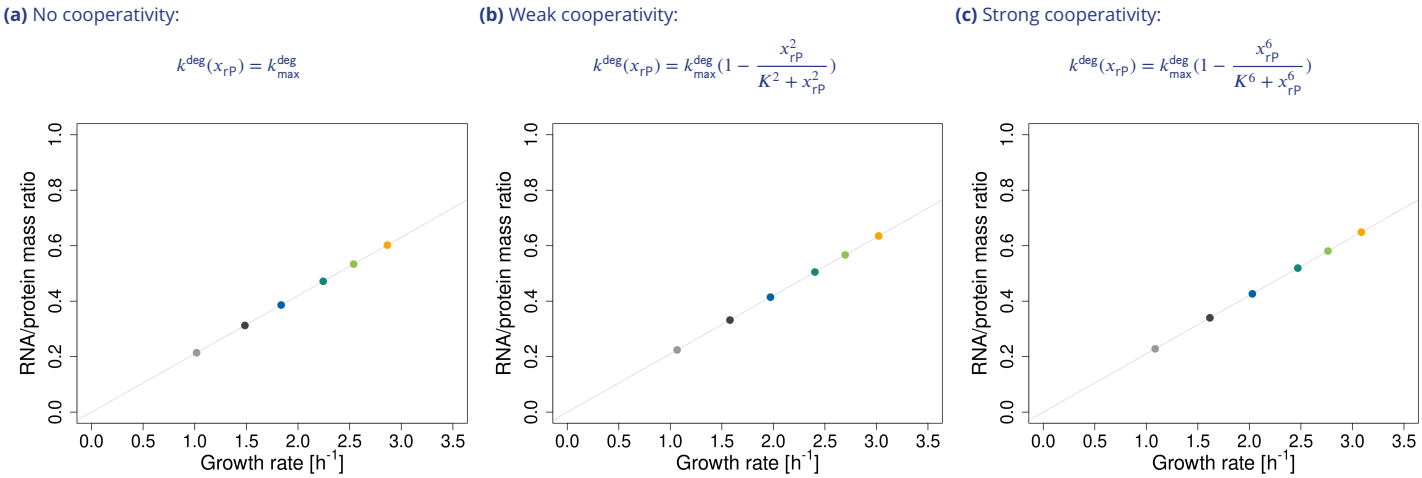

Appendix 1 Figure 3. Our model recapitulates linear relationship of RNA/protein mass ratio and growth rate for all three forms of rRNA degradation function. The points are predicted RNA/protein ratios for *E. coli* in six different conditiosn. The lines are linear fits.

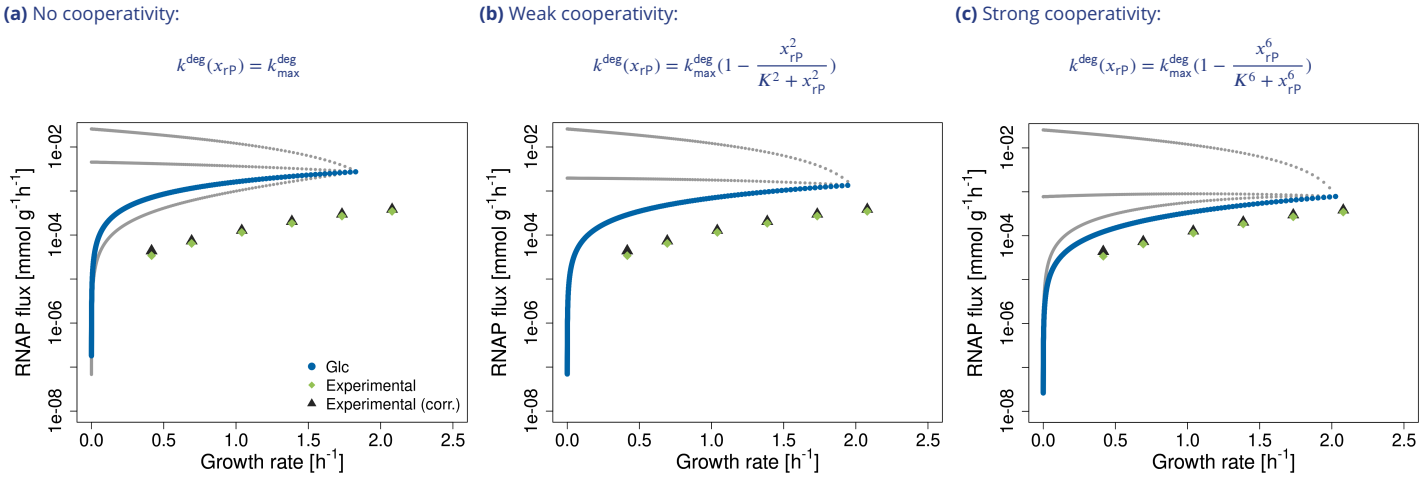

Appendix 1 Figure 4. RNAP fluxes as functions of growth rate for glucose minimal medium. Gray and blue lines are simulations. Light green diamonds are experimental data from ***Bremer and Dennis*** (***2008***), and black triangles are data from ***Bremer and Dennis*** (***2008***) corrected for rRNA degradation (***Gausing, 1977***). Data were converted to $\mathrm{mmol\,g^{-1}\,h^{-1}}$ with *E. coli* dry masses from ***Bremer and Dennis*** (***2008***).

Unlike in the base model (***Figure 2b***), we observe four instead of three alternative solutions (EGVs). The top gray trajectory represents solutions where RNase activity is higher than the enforced minimum given by Eqn. (5), which leads to increased RNAP flux. The middle gray trajectory are solutions where ribosomes accumulate in excess of what is needed for growth. This also increases rRNA degradation via equation (5) and therefore RNAP fluxes. Finally, the bottom gray solutions accumulate rRNA. Blue corresponds to EGVs where rRNA and ribosomes are not accumulating and rRNA is not degraded in excess, that is, constraints “rRNA”, “cap R” and “min deg” in ***Table 1*** are fulfilled with equality.

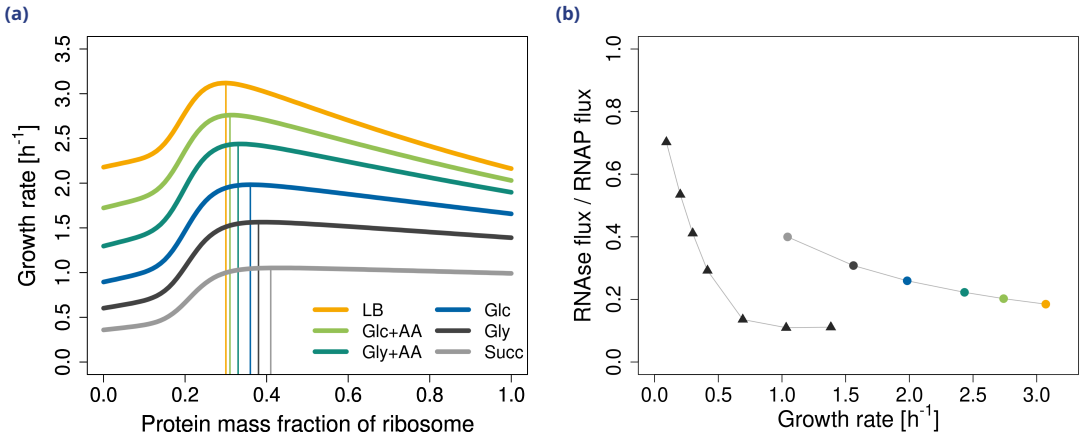

Appendix 1 Figure 5. Accounting for RNAP allocation improves predictions of RNase fluxes. RNAP allocations were included in the model by using the effective transcription rate $\bar{k}^{\mathrm{el}}_{\mathrm{RNAP}} = k^{\mathrm{el}}_{\mathrm{RNAP}} f^{\mathrm{act}}_{\mathrm{RNAP}} \phi^{\mathrm{RNAP}}_{\mathrm{rRNA}}$. The values for $\phi^{\mathrm{RNAP}}_{\mathrm{rRNA}}$ are: Succ, 0.18; Gly, 0.28; Glc, 0.42; Gly+AA; 0.52, Glc+AA, 0.6; LB, 0.65. The values of the other parameters are in ***Table 2***. **(a)** Maximum growth rate for *E. coli* in six different conditions. **(b)** Ratio of RNA degradation to RNA transcription (RNAse flux/RNAP flux) The circles are the predicted ratios of RNAse fluxes to RNAP fluxes at different conditions. The triangles represent experimental data from ***Gausing*** (***1977***) (extracted from the original plot with WebPlotDigitizer (***Rohatgi, 2022***)).

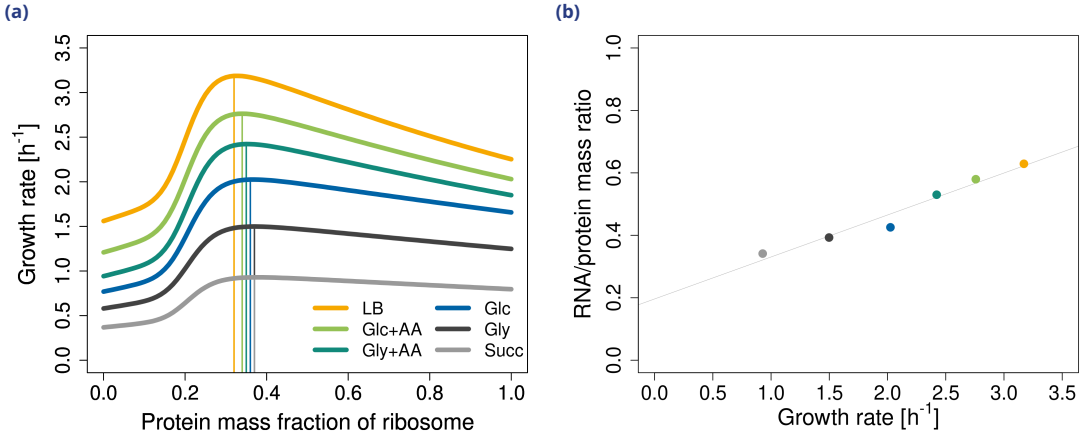

Appendix 1 Figure 6. Variable translation elongation rate has no impact on the predicted optimal ribosome composition, but it leads to a non-zero offset of RNA/protein ratio at zero growth rate. **(a)** Maximum growth rate for *E. coli* in six different conditions. The translation elongation rates ($k^{\mathrm{el}}_{\mathrm{R}}$) are: Succ, 12; Gly, 16.83; Glc, 21 ; Gly+AA, 20.17; Glc+AA, 21; LB, 22.25 $\mathrm{AA\,s^{-1}}$. The remaining parameters are listed in ***Table 2***. **(b)** The points are the predicted RNA/protein ratios in six different conditions. The line is a linear fit.